Lehigh University
Lehigh Preserve

Theses and Dissertations

2016

Electric field-induced softening of alkali silicate glasses

Charles Thomas McLaren
Lehigh University

Follow this and additional works at: http://preserve.lehigh.edu/etd

 Part of the Materials Science and Engineering Commons

Recommended Citation
McLaren, Charles Thomas, "Electric field-induced softening of alkali silicate glasses" (2016). *Theses and Dissertations*. 2723.
http://preserve.lehigh.edu/etd/2723

This Thesis is brought to you for free and open access by Lehigh Preserve. It has been accepted for inclusion in Theses and Dissertations by an authorized administrator of Lehigh Preserve. For more information, please contact preserve@lehigh.edu.

Electric field-induced softening of alkali silicate glasses

By

Charles McLaren

A Thesis

Presented to the Graduate and Research Committee

of Lehigh University

in Candidacy for the Degree of

Master of Science

in

Materials Science and Engineering

Lehigh University

May 2016

© Copyright 2016 by Charles Thomas McLaren

All Rights Reserved

Certificate of Approval

This thesis is accepted and approved in partial fulfillment of the requirements for the Masters of Science.

_____

Date

_____

Himanshu Jain, Thesis Advisor

_____

Helen M. Chan, Chairperson of Department

Acknowledgements

I would like to thank Professor Himanshu Jain for giving me the opportunity to continue my education and to be a part of this research project. I greatly appreciate his guidance and the knowledge I have gained from him so far in my graduate career.

I am grateful to Professor Rishi Raj at the University of Colorado at Boulder for allowing me to visit his laboratories on a research exchange. The technical discussion with him and his graduate student Riccardo Tessarollo were instrumental to the background and setup of this research project.

Thank you to my fellow glass group members Bill Heffner, Chatree Saiyasombat, Adam Stone, Ukrit Thamma, Sean McAnany, Dmytro Savytskyy and Roman Holovchak. Your training sessions, insights, and critical discussions have helped me to advance my laboratory and problem solving skills. I also give a special thank you to Christie Hasbrouck for her help with the experiments. To the rest of the graduate students in the Materials Department thank you for your support and friendships.

I would also like to thank the many members of the Materials Science and Engineering Department. The guidance and assistance of Sarah Wing, Janie Carlin, Lisa Arechiga, Sue Stetler, Katrina Kraft, Laura Moyer, Mike Rex and John Gregoris have played a critical role in assuring the success of this research project.

I am enormously thankful to my family for all of their love and support throughout my education. The encouragement I have received from my parents, grandparents, and siblings has allowed me to achieve all that I have set my mind to.

Finally, I gratefully acknowledge the financial support of the National Science Foundation through the International Materials Institute for New Functionality in Glass (DMR 0844014) at Lehigh University.

Table of Contents

List of Tables

List of Figures

Abstract

Motivated by the advantages of two-electrode flash sintering over normal sintering, we have investigated the effect of an external electric field on the viscosity of glass. The results show remarkable electric field-induced softening (EFIS) as application of DC field significantly lowers the softening temperature of glass. To establish the origin of EFIS, the effect is compared for single vs. mixed-alkali silicate glasses with fixed mole% of the alkali ions such that the mobility of alkali ions is greatly reduced while the basic network structure does not change much. Sodium silicate and lithium-sodium mixed alkali silicate glasses were prepared by standard melt-quench method. The samples were tested mechanically *in situ* under compression in external electric field ranging from 0 to 250 V/cm in specially designed equipment. A creep tester was modified to track viscous displacement of glass while a measurement circuit was built to record voltage across and current though the sample. The circuit was designed to carefully measure current within six orders of magnitude. A comparison of data for different compositions indicates a complex mechanical response due to Joule heating, electrolysis, dielectric breakdown and field-assisted viscous flow.

Introduction

1. U. S. glass industry

Glass manufacturing is energy intensive and often encompasses long processing times. The manufacturing process includes multiple stages which are vital to production of quality articles. The glass melting stage is the most energy intensive and consumes approximately 50-80% of energy costs.[1] While there are many measures to reduce energy consumption of the melting stage, it is still important to note that much of the remaining energy consumption (20-50%) is in post-melting processes.[2] Reduction of energy consumption for soda-lime container glass melting, when optimized conditions are in-place, appears to be nearing the theoretical limit indicating that further research will only provide relatively small energy savings.[1] As for post-melting processes, the state-of-art techniques are far from optimized when considering their theoretical limits.[1] Therefore, energy savings may be more readily obtained through innovative post-melting operations and techniques rather than optimization of melting alone.

2. Two-electrode sintering

Electric fields, applied with a pair of electrodes can reduce the furnace temperature and sintering time of ceramics.[3-6] The effect falls into two regimes, field assisted sintering (FAST) and flash sintering as seen in Figure 1 as linear shrinkage of the sample with respect to furnace temperature. In FAST, which occurs at low field, sintering is somewhat enhanced and progresses gradually with time.[3] By comparison, at higher fields flash sintering occurs abruptly in just a few seconds when a critical temperature is reached at a given applied external field.[3] Flash sintering is characterized by a power

surge produced by an abrupt increase in conductivity. This feature is well illustrated in Figure 2 where current was observed to increase monotonically with temperature until a power dissipation of ~1 watt was reached. The sintering process became unstable when the applied external electric field was above a threshold value of ~50V/cm as displayed in Figure 2. It has also been reported that an applied DC electric field of similar magnitude to flash sintering had a significant influence on the flow stress of fine-grained Al_2O_3 and MgO.[7] This indicates a dramatic increase in mass transport of ceramics.

The mechanism of flash sintering is controversial. The sudden increase in conductivity produces Joule heating, which has been the first explanation of the flash effect. A recent study[8] using dynamic modeling with non-uniform temperature supports pure Joule heating runaway to be responsible for enhancing the sintering rates. The power dissipation in the sample from electrical heating is given simply by:

$$P = \frac{V^2 A}{\rho L} \qquad \text{(Eq. 1)}$$

where P is thermal power dissipation (watts), V is potential drop (V), A is cross sectional area (cm^2), ρ is resistivity (Ω.cm) and L is the thickness of the sample (cm). However, detailed studies[6, 9] suggest that Joule heating alone may not be sufficient to explain the extreme sintering rates of flash sintering. Joule heating was observed to raise the sample temperature a few hundred degrees above the furnace temperature, however, the temperature reached was still relatively low compared to the temperature necessary to fully sinter a ceramic sample in a few seconds.[6] It was proposed that Joule heating has a synergistic effect with an alternate mechanism. In these studies Joule heating was viewed as being a consequence of Frenkel pair defect nucleation at furnace temperature that

subsequently ionizes into charge neutral defects and electron-hole pairs.[9] The proposed model could potentially explain the greatly enhanced mass transport of sintering along with the observed surge of electrical conductivity in insulating ceramic samples.

Beyond the DC results already mentioned, two-electrode sintering has also been observed under AC fields of similar magnitude at frequencies of both 50 and 1000 Hz.[10, 11] The application of AC fields also revealed two distinct sintering regimes of FAST and flash. The main difference observed between DC and AC fields was the development of microstructure. It was reported that AC fields developed equiaxed grains while DC fields preferentially lead to grain growth in one direction.[11]

3. Electro-thermal poling

Electrical fields are often used in glass processing as electro-thermal poling but the mechanism is not well understood. The experimental setup of electro-thermal poling of glasses has many similarities to that of two-electrode sintering. It is a processing technique that is used for bioactive glasses and optical fibers to enhance biological, physical, chemical properties, and nonlinear optical susceptibility.[12-21] The process involves a glass sample sandwiched between ion-blocking electrodes with a DC potential. It is then heated to some specified temperature below the glass transition temperature (T_g) to allow for significant ionic conductivity.[13] The glass is then cooled down to ambient under the DC potential to 'freeze' ionic displacements towards oppositely charged electrodes. Electro-thermal poling has been reported to cause structural rearrangements in glass such as the creation of an alkali ion depletion layer.[22-24] A consistent structural change following electro-thermal poling is an increase in polymerization of the glassy network in the subsurface region at the anode.[22, 23] Thermally and electric field activated

charge compensations of non-spontaneous structural rearrangements have been under debate. However, it appears that the charge compensation mechanism heavily depends on the electrode/glass interface and testing atmosphere.[22-24] For example, a commercially available borosilicate glass with ~5 mol% alkali content was poled at a temperature of 300°C for 30 mins with 2 kV in a nitrogen atmosphere.[24] A gaseous discharge emission at the silicon anode/glass interface was attributed to the N_2 electronic transitions from furnace atmosphere.[24] Within the alkali depletion layer, molecular oxygen, NO^+ and NO_2 were found as evidence of redox reactions.[24] The electro-thermal poling technique can also be used to imprint the surface of glass. Surface patterns can be imprinted using a patterned anode surface at and below the T_g.[25-27] Local glass softening may also be occurring during electric imprinting.

Motivated by the high energy cost of glass processing and the recently reported reduction of furnace temperatures from two-electrode sintering, it is natural to ask if reduction in furnace temperature for bulk glass softening is possible. An adaptation of two-electrode sintering and electro-thermal poling techniques for bulk glass softening has potential for increased glass processing efficiency.

Here we report on electric field-induced softening (EFIS) phenomenon in glass. The furnace temperature below the conventional softening temperature of glass at which the onset of large displacement or viscous flow of glass occurs is defined as EFIS. The results show that glass softens at furnace temperatures well below T_g under DC electric fields. The softening is accompanied by optical emission.

Experimental Methods

1. Glass compositions and preparation

Two disilicate glass compositions were selected for this study: a single alkali sodium silicate (NS) and two lithium-sodium mixed alkali silicates (2L8NS and 5L5NS). Their composition is listed in Table 1. Owing to the well-known mixed alkali effect these glasses have similar network structure but different DC electrical resistivity.[28] All glasses were made using standard melt quench method starting with a batch of SiO_2 (LTS Chemical Inc., 99.99%), Na_2CO_3 (Alfa Aesar, 99.95%) and Li_2CO_3 (Fisher Scientific, 99.1%) powders. These precursors were weighed in appropriate ratio and mixed thoroughly. The batch was heated in a Pt-Rh crucible and melted at 1550°C for 3 h in an electric furnace. The melt was poured into rectangular stainless steel molds. Samples, from the same batch, were also made by pressing between two stainless steel plates; these were used for electrical impedance measurements. Finally, all samples were stress annealed at 30°C below T_g for 3 h and slowly cooled to room temperature. They were cut to the shape of a rectangular block and polished to a final cross-section of 5 mm x 5 mm and a height of about 10 mm. The grit sizes used, in order, were 240, 320, 400 and 600. A solution of mineral spirits and paraffin wax was used instead of water to avoid alkali ions from being leeched out during sample preparation. Conductive carbon paste was applied to the top and bottom of the sample to ensure good electrical contacts with the graphite electrodes.

2. Characterization methods of glass samples

The glass transition onset temperature (T_g) was determined by differential scanning calorimetry (DSC) in a NETZSCH 404/3F microcalorimeter. The DSC measurements were done from ambient temperature to 800°C at 10°C/min. The values for T_g are reported in Table 1.

Electrical impedance was measured on samples that were ground and polished to obtain parallel surfaces. Gold electrodes were sputtered on the top and bottom of the sample in a three-probe configuration using a Polaron SEM Coating Unit E5100 and a ring mask. A schematic of electrode configuration is shown in Figure 3 along with circuit connections.[29] Figure 4 demonstrates the sample configuration where the top center electrode was connected to high tension, bottom electrode was low tension and top outer ring electrode was ground. Gold electrodes were connected to platinum wires using high purity silver paint. The AC conductance (G) and capacitance (C) of the samples were measured in a frequency range from 10 Hz to 100 kHz using a capacitance bridge (Andeen Model CGA-83), as a function of temperature from ambient up to T_g. Measurements were performed when the temperature was stabilized within ±0.2 K. Impedance spectroscopy testing procedure is provided in Appendix A for use of the Andeen capacitance bridge.

Energy-dispersive X-ray spectroscopy (EDS) was used for chemical analysis using scanning electron microscopy (SEM) (Hitachi 4300SE/N). Samples were coated with iridium to reduce charging effects.

3. Design of EFIS Equipment

A pneumatic creep tester (Applied Test Systems model 2605) shown in Figure 5 was chosen to conduct electric field-induced softening experiments due to its ability to applied a load and contain two window slits into the furnace. Modifications were needed to mechanically test the glass samples under DC electrical fields as seen in Figure 6. Modifications to the furnace included the addition of a cathode and anode to apply an electric field across the sample. A spectrometer probe and video camera used the window slits into the furnace. A thermocouple (TC) was place further into the furnace near the sample. The original design of the ATS pneumatic creep tester was for tension testing only. A set of hooks were designed to take advantage of using tension to create compression (pull to push), as shown in Figure 7, and made in-house as seen in Figure 8. The compressional hooks where placed on the ends of the pull rods as seen in Figure 9a. The sample placement between hooks is displayed in Figure 9b with the sample thermocouple near the sample on the backside of the hooks. An overall schematic of the experimental setup is given in Figure 10. Optical emission was recorded through two window slits in the furnace. The spectrum was recorded with an Ocean Optics USB4000 UV-VIS-ES spectrometer with an optical resolution of ~1.5nm.

4. Measurement of EFIS

A constant heating rate of 10°C/min was used for all samples. Furnace temperature was determined with a thermocouple placed next to the sample where placement is shown in Figure 6. The experiments were carried out under compressive load of 10 MPa. The displacement was measured with an Omega LD621-15 linear variable differential transformer (LVDT) gauge. Electric field-induced softening was

measured by the onset of displacement of the push rod. Measurement of EFIS testing procedure is provided in Appendix B for use of the ATS pneumatic creep tester.

The applied external electric field ranged from 0 to 250 V/cm, with a power supply (Harrison Laboratories model 890A). The electrical behavior of the samples was measured by a specially designed circuit as shown schematically in Figure 11. Voltage was measured across the sample. Current was measured as a voltage across a sensing resistor of either 1 Ω or 1 kΩ which converted the current measurement into a voltage. The voltage across the sample and voltage corresponding to current were recorded using a DATAQ Instruments model DI-149HS. A power resistor of 250 ohm was inserted in series with the sample in order to limit the current in the circuit to 0.5 A.

The voltage across the sample was recorded by stepping down the measured voltage by use of a precision operational amplifier (OP07) by a factor of 100 as shown on the left side of Figure 11. If an AC voltage was used, the measured voltage was then rectified by a second operational amplifier (LM 358A) and a diode (IN4148). Finally, the measured voltage was filtered by the use of a third operational amplifier with two capacitors (2.2 μF feedback capacitor and 0.68 μF capacitor to ground). Following this processing the measured voltage was reduced and filtered to a 0 to 10 V DC signal that was recorded in WinDaq software provided by DATAQ Instruments.

The voltage across the selected sensing resistor was recorded by the processing steps shown on the right side of Figure 11. At low electrical conductivities corresponding to low furnace temperatures, the 1 kΩ sensing resistor was used to multiply the current measurement through the sample. The resistance across the 1 kΩ sensing resistor is

negligible compared to the resistance of the glass sample at low temperatures. At higher electrical conductivities, the 1 Ω sensing resistor was used when lower amplifying gain was needed. This also ensured the resistance across the sensing resistor was again negligible compared to the sample, as the sample resistance decreases with an increase in temperature. The amount of gain was controlled by a rotatory switch with a precision operational amplifier which multiplied the measured voltage across the sensing resistor. The gain was determined by the ratio of the input resistor (10 kΩ) with the selected feedback resistor. The feedback resistors used were 10 MΩ, 1 MΩ, 100 kΩ and 10 kΩ, which are displayed in Figure 11 and correspond to a gain of x1,000, x100, x10 and x1, respectively. The rotary used for controlling gain was a 2-pole 6-position switch. This allowed for the opportunity to record the switch position of the gain by following an incremental voltage drop across series resistors on the second pole. A switch was installed where if AC experimental conditions were used, the measured voltage across the sensing resistor could be rectified into a DC signal similar to how the voltage across the sample was processed. If the experimental conditions were for DC, then the switch could be changed to skip this step. Finally, the measured voltage was filtered to eliminate noise captured by the circuit that could be amplified by the precision operational amplifier. The processed signal was recorded within 0 to 10 V DC and in the same WinDaq software.

The recorded voltage drop across the sample and the voltage across the sensing resistor corresponding to the current were imported into Microsoft Excel. Here, a template was used to adjust the processed voltage and current signals to accurate values. The template simply multiplied the voltage signal by a factor of 100 to adjust the processed voltage value to match the applied voltage. Since further processing went into

recording the current through the sample, the following equation was used to adjust the recorded voltage corresponding to the current through the sample as:

$$I = \frac{V_I - B}{R_S * G} \quad \text{(Eq. 2)}$$

where I is the current through the sample [A], V_I is the voltage across the sensing resistor [V], B is the baseline voltage of the measurement circuit [V], R_S is the resistance of the sensing resistor [Ω] and G is the gain of the operational amplifier [unitless]. This template was also used to simultaneously record run time, push rod displacement (1V/mm), gain switch position, applied load (voltage = 0.01*load + 0.3 [V]) and furnace temperature (100°C/V).

Videos of EFIS were also recorded through the front window slit into the furnace. The videos were captured with a frame rate of 29 frames per second. The time stamp of the videos was synchronized to the run time recorded by the DI-149HS using Logger Pro 3.8 provided by Vernier Software.[30] The video recording was started upon the observation of small photoemissions near the anode and was stopped after the glass was fully displaced and the applied external electric field was removed.

Results & Discussion

1. Characterization of glass samples

The glass transition temperature was measured for each batch of glass made for each composition. This was done to ensure each glass batch was similar to reduce variation in the results. The T_g for NS was measured to be 475°C as shown in Figure 12. The mixed alkali glasses 2L8NS and 5L5NS had T_g values at 427 and 418°C, respectively. A representative run for 2L8NS is shown in Figure 13 while 5L5NS is displayed in Figure 14.

Impedance spectroscopy was used to characterize the electrical behavior of each glass composition. The AC conductance (G) and capacitance (C) of each composition were measured using the capacitance bridge. Complex impedance analysis of G and C yielded DC conductivity as a function of temperature. Complex impedance analysis is composed of calculating the real (Z', in phase resistance) and imaginary (Z", out of phase resistance) parts of electrical impedance ($Z = Z' + iZ''$). The real and imaginary impedance are determined by the following relations:

$$Z' = \frac{G}{G^2+\omega^2C^2} \quad \text{(Eq. 3)}$$

$$Z'' = \frac{\omega C}{G^2+\omega^2C^2} \quad \text{(Eq. 4)}$$

where ω is angular frequency [Hz]. The intersection of Z" vs. Z' on the Z' axis at low frequencies gives the inverse DC conductance $1/G_{DC}$. The DC conductivity is then calculated from the G_{DC} by multiplying by geometric factors of the sample shown in Figure 3 where g is the guard ring thickness, r_1 is central electrode radius and d is the

sample thickness to give $\sigma_{DC} = G_{DC}d/\pi r_1$. Representative measurements for conductance and capacitance are shown in Figure 15 and Figure 16 for the 2L8NS glass composition, respectively. The conductance and capacitance measurements followed similar behavior for NS and 5L5NS compositions. The measured conductance and capacitance data, as shown in Figure 15 and Figure 16 were then used to calculate complex impedance using Eq. 3 and Eq. 4. The complex impedance was then used to create a Nyquist plot for the imaginary impedance Z" vs. the real impedance Z' as a function of temperature as seen in Figure 17 for 2L8NS.

2. Electric field-induced softening

Representative behavior of glass softening is shown in Figure 18, in terms of the displacement (shown as negative values since the experiments were one in compression) as a function of temperature (experiments were done at a constant heating rate). These data are for the NS glass. Results from several samples each tested at a certain applied field are reported. The fields were varied from 0 to 200 V/cm. Representative softening behavior of 2L8NS is shown in Figure 19 while 5L5NS is shown in Figure 20.

There is a slight displacement in the push rod as the temperatures rises, which is attributed to thermal expansion in the loading structure as demonstrated by using an alumina sample in Figure 18. The greater displacement at higher temperatures indicates viscous flow. We define the softening temperature, T_s, by the abrupt onset of large deformation indicated by the red arrow in Figure 18. Note that the temperature for the onset of viscous flow decreases as the applied electrical field is increased.

The curves 0, 50 and 100 V/cm field of NS show compressive displacement that occurs gradually. But at fields greater than 125 V/cm viscous flow occurs abruptly. (A visual demonstration is included in a video as supplemental information). Thus we observe two regimes of behavior. At low electric fields (≤100 V/cm in Figure 18, stage I) the viscosity decreases gradually, in a manner that is similar to the reference sample at 0 V. However, at high fields (≥ 125 V/cm, stage II), NS samples flow quickly, within a few seconds, at furnace temperatures that are well below T_g (see Figure 18 below for details). This behavior is similar to the observations in flash sintering experiments with ceramics.[3] However, when the glass composition is changed to a mixed alkali glass, the phenomenon still occurs but it does not have as pronounced of an effect on reduced softening as revealed by Figure 19 for 2L8NS and Figure 20 for 5L5NS.

The effect of glass composition is analyzed by normalizing the data with respect to T_g. These results are included in Table 1. The normalized EFIS effect can be quantified with parameter $\Delta T(V) = (T_{s0}-T_{sV})$, where T_{s0} is the softening temperature at 0 V, and T_{sV} the softening temperature under an applied field. These results, shown in Figure 21, delineate two regimes of behavior (stage I and II) similar to FAST and flash sintering in ceramics. At low electric fields, in stage I, $\Delta T(V)$ is small and increases slightly with field. At higher fields, typically above a threshold value, $\Delta T(V)$ begins to increase rapidly, marking a transition from stage I to stage II. For NS, 2L8NS and 5L5NS the threshold fields are approximately 95, 100 and 175 V/cm, respectively. Above the threshold, the value of $\Delta T(V)$ is significantly higher for the binary NS glass than for the mixed alkali glasses. From Figure 21, $\Delta T(V)$ for NS had a maximum value of about 150°C while 2L8NS and 5L5NS $\Delta T(V)$ values were only about 50 and 25°C,

respectively. This effect is attributed to the higher resistivity of the mixed alkali glasses. A higher resistivity reduces Joule heating, as shown by Eq. (1), which may be responsible for the lower values of $\Delta T(V)$. It is not clear why $\Delta T(V)$ for the NS glass increased continually with applied field, whereas it reaches a plateau at ~175 V/cm for the mixed alkaline glasses.

The relationship between the current flowing through the sample and viscous flow, for the NS glass at 175 V/cm, is shown in Figure 22. Before softening, the current rises steadily with temperature as expected from increased ionic conductivity. Prior to EFIS, small spikes in the current measurement are observed. A few of these current spikes can be seen in Figure 22 where there will be a brief jump in current and return to a value similar to before the spike. At the onset of field induced softening the current rises sharply. The high conductivity of the sample is evident from the equally sharp drop in voltage. This behavior is similar to the experience in flash sintering where the power supply was switched from voltage to current control when the current rises abruptly.[4] In the present experiments the current was limited by the 250 ohm resistor placed in series with the sample.

Prior to the high current regime of EFIS, it is believed that the glass behaves similarly to electro-thermal poling processing. It has been reported[12-14, 16] that current during electro-thermal poling is due to ionic transport of alkali ions, which forms an alkali depletion layer in the glass near the anode. As the depletion layer forms, a greater amount of the applied electric field drops across this layer. It occurs due to the increasing removal of alkali ions causing the depletion layer resistance to increase. This results in an increase of the local electric field near the anode which can reach approximately to the

order of 10^7 V/cm, which is close to the dielectric strength of silicate glasses.[13] This process has recently been outlined by Zakel et al.[13], for a bioactive glass.

3. Joule heating

In industry, Joule heating is used for melting and fining of glass.[31, 32] This technique depends on glass resistivity and its temperature dependence. So we ask if EFIS is simply due to Joule heating. DC resistivity was determined from AC complex impedance analysis with a value of 3.88×10^8 Ω.cm for NS, 1.19×10^{11} Ω.cm for the 2L8NS and 9.49×10^{11} Ω.cm for 5L5NS at room temperature. The activation energy for DC electrical conductivity for each glass composition was calculated by fitting the temperature dependent data to the Arrhenius equation as follows:

$$\sigma_{DC} = \frac{A}{T} \exp\left(-\frac{E_a}{kT}\right) \quad \text{(Eq. 5)}$$

where T is temperature [K], E_a is activation energy [eV], k is Boltzmann's constant [eV/K] and A is a pre-exponential fitting parameter. The corresponding activation energies for NS, 2L8NS and 5L5NS were calculated from Arrhenius plot given in Figure 23 as 0.69, 0.92 and 0.97 eV, respectively. These values are in good agreement with literature values of similar compositions as NS, 2L8NS and 5L5NS which were 0.63, 0.96 and 1.01 eV, respectively.[33]

Multiple videos of experiments showed evidence of fuming, which was accompanied by buildup of white powder on the push rods. Buildup of white powder was observed on the compression hook near the anode as observed in Figure 24a. Powder was collected after an experimental run of 2L8NS with 200 V/cm and investigated using EDS where spot 1, Figure 24b, is indicated by the red crosshairs with its collected spectrum,

Figure 24c. A second spot was analyzed in Figure 24d and again indicated by the red crosshairs with its collected spectrum, Figure 24e. The semi quantitative compositions are given in Table 3. The powder from 2L8NS at 200V/cm was revealed to be consistent as glass that had condensed on the surfaces during cooling. No additional EDS peaks were observed outside of the glass composition. This is unexpected behavior since these glass compositions should not vaporize even with the higher specimen temperature as estimated from Joule heating, see below. Evidently, much higher temperatures were reached in the depletion layer next to the electrodes[12, 13] which would have caused vaporization.

As a rough approximation, Joule heating can be estimated as the power dissipated within the sample during EFIS. The power dissipation can be estimated using the voltage across the sample with the current passed as follows:

$$Q = \int_{t_s}^{t_f} v * I \, dt \qquad \text{(Eq. 6)}$$

where Q is the thermal energy due to power dissipation [J], v is the voltage across the sample [V], I is the current [A], t_s and t_f are the start and finish times of EFIS [sec]. This assumes complete conversion of electrical energy into thermal energy. The thermal energy estimated from Eq. 6 can then be used to calculate a corresponding temperature rise within the sample as simple heat transfer with the following relation:

$$Q = m * C_p * \Delta T \qquad \text{(Eq. 7)}$$

where m is the mass of the sample [g], C_p is the specific heat capacity of the glass [J/g.K], and ΔT is the change in temperature from initial to final [K]. For example, we consider NS with 175 V/cm applied as shown in Figure 22 we get an estimated

temperature increase of about 760°C during EFIS. This estimate neglects heat loss due to thermal conduction during this brief period. The furnace temperature at the time EFIS occurred was about 425°C leading to an overall sample temperature of about 1185°C. This temperature estimate certainly accounts for glass softening but not vaporization of glass. However, with localization of heat to the depletion layer the actual temperature rise could be considerably higher, enough to account for melting and vaporization. Lack of information on the depletion layer makes the determination of actual temperature at present difficult.

4. Photoemission Spectra

Just prior to and during EFIS each glass composition produced photoemission at fields greater than 50 V/cm. Figure 25a. shows NS sample under 150 V/cm field at a furnace temperature of ~435°C before photoemission. When the temperature was increased above the flashing temperature (T_F), the first photoemission and accompanying current spike were observed as seen in Figure 25b for a furnace temperature $T_F < T < T_{sV}$ (for details see the video in supplemental information). Measurements of optical emission from the specimen correlated with the current spikes. Figure 25b visually captured the photoemission near the anode. When the recorded data was synchronized with the video, it was observed that the glass samples would flash during the current spikes and sustained high current shown in Figure 22. This marks high conductance of the material which suggests dielectric breakdown of the glass presumably across the depletion layer via electron avalanche. It has been observed that NS flashed for a longer time frame (~2-5 min) before EFIS, while 2L8NS flashed for about a minute or less before EFIS.

The photoemission spectra for NS and 2L8NS are shown in Figure 26. The photoemission spectra for the two compositions are similar, with a broad background in the visible and near-infrared region and several sharp characteristic peaks. All samples show an intense emission peak at ~589 nm. In the presence of lithium, in 2L8NS, two additional peaks at 611 and 671 nm are observed. The peak energies match very well with the electron energy level transitions for the alkali ions, as in Grotrian diagrams provided by NIST.[34] The sharp peaks suggest photoemission from gaseous species as opposed to electroluminescence reported for stage III flash sintering of yttria stabilized zirconia as exciton recombination.[35] A comparison of the photoemission peaks is presented in Table 2 for NS and 2L8NS at 200 V/cm. An impurity peak located at 767 nm is identified using EDS as due to potassium that is present as an impurity similar to that has been seen in the spectra of high pressure sodium vapor lamps.[36-38] The observed photoemission peaks follow a behavior similar to breakdown conduction of Al-SiO-Al, Al-SiO-Ni and Al-MgF_2-Al capacitors as well.[39]

The large broad background in the optical emission has been identified as bremsstrahlung radiation. This indicates electrons are undergoing deceleration in the Coulombic field of the atoms.[40] The current spikes are believed to be related to an electron avalanche breakdown process.[39] The bremsstrahlung radiation has a short wavelength limit, which is the maximum energy of a single collision event within the sample. The highest energy observed can be estimated by the short-wavelength limit as shown by Goldstein.[40] An estimate for the spectra shown in Figure 26 for 200 V/cm is approximately at 460 nm which corresponds to a maximum energy value of an electron at about 2.70 eV.

The identified mechanisms responsible for EFIS should be related to those of electro-thermal poling since glass samples are processed similarly. The main difference between EFIS and poling appears to be that the glass is taken to conditions that are viable for dielectric breakdown to occur. It has been proposed that during electro-thermal poling, electrons are injected into the conduction band of the glass from the cathode towards the anode for charge compensation.[13] These electrons would then migrate towards the anode, and get accelerated upon reaching the depletion layer due to the presence of an extremely high potential drop. It is conceivable that electrons such as at the non-bridging oxygen atoms are also injected from the region next to the depletion layer. At this field strength, which can be close to the critical field strength, impact ionization may result from electron avalanche across the depletions layer. Since bremsstrahlung radiation is indicative of electron-generated radiation, the accelerated electrons are presumed to collide with alkali ions migrating towards the cathode. These interactions can also excite and relax discrete energy levels within alkali ions, creating characteristic photoemission peaks.

Summary

A new phenomenon of electric field induced softening (EFIS) of glass has been identified. The application of electric field produces glass deformation at low furnace temperature. A higher field continues to reduce the furnace temperature for the onset of softening. The EFIS effect is stronger for the single than for the mixed alkali silicate glasses, suggesting a role for ionic mobility in this phenomenon. The results suggest the following mechanism: The application of DC field during heating forms an alkali ion depletion layer near the anode. Joule heating within the sample becomes significant at higher temperatures as ionic conductivity increases overcoming heat dissipation. An electron avalanche occurs over the depletion layer resulting in photoemission comprising of bremsstrahlung radiation and characteristic alkali ion electron energy level peaks. These processes create a positive feedback system of Joule heating, charge injection, space charge formation and electrolysis resulting in glass softening, melting and ultimately vaporization.

Future Work

1. **Glass compositions**

A continuation of the glass compositions of NS, 2L8NS, 5L5NS and LS from Table 1 along with a sodium aluminosilicate (70 mol% SiO_2, 25 mol% Na_2O, 5 mol% Al_2O_3, NAS) will be used for future experiments for comparison of model glass systems. Glasses will be made using standard melt quench method as used for completion of the Master's Thesis.

2. **EFIS quantification**

Further investigation of EFIS quantification is needed in order to observe how glass is influenced by processing parameters. Two important parameters that have not been fully explored are pressure dependence and AC frequency dependence of EFIS. Both parameter behaviors are crucial to knowing how to tailor the phenomenon for process optimization. Thesis work has only used pressure as a probe for glass softening which also provided force to ensure good electrical contact between the electrodes and the glass. The NAS glass type will be used to investigate pressure dependence ranging from an applied load of 0.5 to 50 MPa during a standard EFIS experimental run. An AC frequency of 60 Hz with 120 V has only been used as preliminary data to this point and was similar to a DC field. To purely study the effect of AC frequency, the heating rate and applied voltage will remain constant (10°C/min & 120 V/cm) while testing a wide range of frequencies from 10 Hz – 100 kHz on NS, 2L8NS, 5L5NS and LS glasses.

3. Identification of mechanisms

Electric field-induced softening is a complex mechanical response of alkali silicate glasses to several mechanisms. The current work has proposed several possible mechanisms however, more experimental data and modeling are needed for confirmation. Similar techniques such as electro-thermal poling of alkali silicate glasses may provide much greater insight on mechanisms involved. Joule heating remains as the leading mechanism to EFIS at higher temperatures where resistive heating occurs faster than heat dissipation and convection. Thus, incubation experiments are needed to provide insight on the time dependence of thermal runaway at a constant furnace temperature. Experimental parameters that will be varied include isothermal hold temperatures, applied electric field magnitude and type (AC and DC). The isothermal temperature will determine the ionic conductivity of the glass samples already known from impedance spectroscopy and activation energy calculations from preliminary work. A variation in the applied electric field magnitude will influence the depletion layer thickness which will ultimately determine the number of broken NBOs created. A change in glass composition will help delineate the role of Joule heating from other possible EFIS mechanisms due to differences in resistivities of the mixed alkali disilicate glasses.[28] These glasses also provide an advantage since they have similar thermal conductivities yet will produce Joule heating differently.[33] Samples will be cooled at various stages under an applied field after an incubation period to preserve the chemical and structural environments of the glass.

Electro-thermal poling techniques will also be used in order to gather information about mechanisms on the formation of an alkali depletion layer near the anode. The

samples tested provide valuable information about the electrical behavior of glass with DC electric field prior to dielectric breakdown as observed with EFIS. Impedance spectroscopy will be used in situ with electro-thermal poling to characterize the DC resistivity, capacitance and thickness of the depletion layer as a function of poling time at an isothermal temperature. Separate poling experiments will investigate the time dependence of current decay. Current measurements will provide relaxation time constants of possible polarization and electrolysis mechanisms. Time-of-flight secondary ion mass spectroscopy (TOF-SIMS) will then be used for chemical analysis post-mortem by use of sputtering to create a depth profile from each electrode interface into the bulk of the glass. Finally, since electro-thermal poling is primarily conducted as an isothermal hold, thermally stimulated poling (TSPC) and depoling (TSDC) currents will be tests on each glass composition to relate poling experiments to EFIS. These techniques will provide estimates for activation energy for ionic species motion and charge compensation mechanisms during a constant heating rate.

Recently, the measuring circuit used to record current and voltage of EFIS has been upgraded to the point where thermally stimulated poling (TSPC) and depoling (TSDC) current measurements within the existing ATS furnace should be possible. Again, the samples will be cooled at various segments of the run to room temperature under the applied electric field to preserve the structural and chemical state of the glass. Evidence of treeing/branching of high current paths through the bulk of the sample characteristic of dielectric breakdown will be examined.[39] Identification of the chemical state of the glass using XPS at various states of EFIS are still needed. Depth profiling using LEIS will be done on the same samples used for XPS to investigate alkali ion

migration. Information gained from XPS and LEIS will then be compared to structural data collected from microRaman. Mapping of structural changes will be possible by microRaman along the cross section of quenched samples.

A feature of EFIS in Fig. 4 that has not been accounted for yet is the plateaued EFIS effect for the mixed alkali glasses. The resistivities of the mixed alkali glasses (2L8NS and 5L5NS) are much greater than for NS by about 3 orders of magnitude. In general, the resistivity is related to the electric field by current density. Since the resistivity of the mixed alkali glasses is much greater, the relatively small increase in electric field magnitude will not create a large change in current density. An initial hypothesis is that much greater electric field strength is needed for current density of the mixed alkali glasses to match that of NS. If this is true, then this result would support Joule heating as the main mechanism of EFIS. However, NS should also be tested at higher applied electric field magnitudes to investigate whether it has a plateau similar to that of mixed alkali glasses. This result will indicate if the depletion layer depth and accompanying resistivity reaches saturation with diminishing EFIS effect supporting the notion of a preceding mechanism to Joule heating.

4. EFIS finite element modeling

Finite element analysis (FEA) will be used to gain insight on both uniform and non-uniform Joule heating scenarios during EFIS. Analysis will be done using Abaqus 6.13 software which allows for coupled thermal-electrical-structural element calculations.[41, 42] A uniform Joule heating scenario will be investigated first to gain general information about power dissipation and heat conduction within glass samples. However, this model is not a good comparison to EFIS due to the formation of a

depletion layer near the anode. This depletion layer will both grow in thickness and resistivity during an experiment greatly influencing Joule heating. During the high current regime of EFIS, the depletion layer will become electronically conductive and no longer be the dominant source of Joule heating compared to the bulk of the sample. Therefore, it is predicted that a non-uniform Joule heating model will produce more realistic estimates of EFIS. These data and model will then be used for comparison of measured data and flash sintering modeling[6, 8] to gain insight on the role of various mechanisms and parameters involved with EFIS of alkali silicate glasses.

References

1. K. Bange, H. Jain and C. Pantano, Making Glass Better, 1st edn. (International Commission on Glass, Madrid, 2015), p. 55.

2. C. P. Ross and G. L. Tincher, Glass Melting Technology: A Technical and Economic Assessment, 1st edn. (Glass Manufacturing Industry Council, Westerville, 2004), p. 32.

3. M. Cologna, B. Rashkova and R. Raj, J. Am. Ceram. Soc. 93, 3556 (2010).

4. K. S. Naik, V. M. Sglavo and R. Raj, J. Eur. Ceram. Soc. 34, 2435 (2014).

5. M. Cologna, John S. C. Francis and R. Raj, J. Eur. Ceram. Soc. 31, 2827 (2011).

6. R. Raj, J. Eur. Ceram. Soc. 32, 2293 (2012).

7. H. Conrad, Scripta mater. 44, 311 (2001).

8. R. I. Todd, E. Zapata-Solvas, R. S. Bonilla, T. Sneddon and P. R. Wilshaw, J. Eur. Ceram. Soc. 35, 1865 (2015).

9. K. S. Naik, V. M. Sglavo and R. Raj, J. Eur. Ceram. Soc. 34, 4063 (2014).

10. M. C. Steil, D. Marinha, Y. Aman, J. R. C. Gomes and M. Kleitz, J. Eur. Ceram. Soc. 33, 2093 (2013).

11. C. Schmerbauch, J. Gonzalez-Julian, R. Röder, C. Ronning and O. Guillon, J. Am. Ceram. Soc. 97, 1728 (2014).

12. C. R. Mariappan and B. Roling, J. Non-Cryst. Solids 356, 720 (2010).

13. J. Zakel, M. Balabajew and B. Roling, Solid State Ionics 265, 1 (2014).

14. E. C. Ziemath, V. D. Araújo and C. A. Escanhoela, J. Appl. Phys. 104, 054912 (2008).

15. A. L. Moura, M. T. de Araújo, E. A. Gouveia and M. V. D. Vermelho, Optics Express 15, 143 (2007).

16. C. M. Lepienski, J. A. Giacometti, G. F. Leal Ferreira, F. L. Freire Jr. and C. A. Achete, J. Non-Cryst. Solids 159, 204 (1993).

17. J. Zakel, V. Heddinga, S. O. Steinmüller and B. Roling, Solid State Ionics 237, 46 (2013).

18. C. R. Mariappan and B. Roling, Solid State Ionics 179, 671 (2008).

19. J. Kruempelmann, C. R. Mariappan and B. Roling, Phys. Rev. B 82, 224203 (2010).

20. U. K. Krieger and W. A. Lanford, J. Non-Cryst. Solids 102, 50 (1988).

21. André Luiz Ribeiro Brennand, 1 (2002).

22. M. Dussauze, V. Rodriguez, A. Lipovskii, M. Petrov, C. Smith, K. Richardson, T. Cardinal, E. Fargin and E. I. Kamitsos, J. Phys. Chem. C 114, 12754 (2010).

23. N. Smith and C. Pantano, Appl. Phys. A 116, 529 (2014).

24. T. Cremoux, M. Dussauze, E. Fargin, T. Cardinal, D. Talaga, F. Adamietz and V. Rodriguez, J. Phys. Chem. C 118, 3716 (2014).

25. N. Ikutame, K. Kawaguchi, H. Ikeda, D. Sakai, K. Harada, S. Funatsu and J. Nishii, J. Appl. Phys. 114, 083514 (2013).

26. S. Youn, H. Takagi, S. Park, M. Takahashi and R. Maeda, J. Nanosci. Nanotechnol. 12, 3181 (2012).

27. A. Lipovskii, M. Kuittinen, P. Karvinen, K. Leinonen, V. Melehin, V. Zhurikhina and Y. Svirko, Nanotechnology 19, 415304 (2008).

28. D. E. Day, J. Non-Cryst. Solids 21, 343 (1976).

29. H. Jain, in Experimental Techniques of Glass Science, edited by C. J. Simmons and O. H. El-Bayoumi (American Ceramic Society, 1993), Chap. Measurement of Electrical Conductivity of Glasses, pp. 433-461.

30. Vernier Software, Version 3, http://www.vernier.com/products/software/lp/ (2009).

31. C. F. De Voe, U.S. Patent No. 2,490,339 (Dec. 6, 1949).

32. J. Stanek and J. Matej, J. Non-Cryst. Solids 84, 353 (1986).

33. N. P. Bansal and R. H. Doremus, Handbook of Glass Properties, (Academic Press, Inc., Orlando, 1986), p. 381-449.

34. C. E. Moore and P. W. Merrill, NSRDS National Bureau of Standards 23, (1968).

35. K. Terauds, J-M Lebrun, H. H. Lee, T. Y. Jeon, S. H. Lee, H. J. Je and R. Raj, J. Eur. Ceram. Soc. 35, 3195 (2015).

36. J. J. de Groot and J. A. J. M. van Vliet, The High-Pressure Sodium Lamp, 1st edn. (MacMillan Education LTD, London, 1986), p. 23.

37. M. Rakić and G. Pichler, Optics Communications 284, 2881 (2011).

38. C. D. Elvidge, D. M. Keith, B. T. Tuttle and K. E. Baugh, Sensors 10, 3961 (2010).

39. Paul P. Budenstein, IEEE Transactions on Electrical Insulation EI-15, 225 (1980).

40. J. Goldstein, D. Newbury, D. Joy, C. Lyman, P. Echlin, E. Lifshin, L. Sawyer and J. Michael, Scanning Electron Microscopy and X-Ray Microanalysis, 3rd edn. (Springer, New York, 2007), p. 271-296.

41. S. Y. Hilali and B. J. Wang, ABAQUS Users' Conference May, 441 (1995).

42. B. J. Wang and S. Y. Hilali, ABAQUS Users' Conference May, 771 (1995).

Tables and Figures

Table 1. Glass compositions and their respective T_g and T_{s0} values.

Glass type	Glass Composition	T_g [°C]	T_{s0} [°C]
NS	$0.3Na_2O•0.7SiO_2$	475	550
2L8NS	$0.33[0.2\ Li_2O•0.8Na_2O]•0.67SiO_2$	427	491
5L5NS	$0.33[0.5\ Li_2O•0.5\ Na_2O]•0.67\ SiO_2$	423	493

Table 2. Peak centers of the 2L8NS photoemission during 200 V/cm test condition as seen in Figure 26. The peak centers were matched to alkali ion electron energy level transitions.[34]

200 V/cm electron energy level transition table					
Peak Label	Peak Center (nm)	Peak Energy (eV)	Transition[34]	Transition Energies[34] (eV)	Transition Energy Difference (eV)
A	499	2.48	Na I 5d to 3p	4.59-2.10	2.49
B	569	2.18	Na I 4d to 3p	4.28-2.10	2.18
C	589	2.10	Na I 3p to 3s	2.10-0	2.10
D	592	2.09	Na I 3p to 3s	2.10-0	2.10
E	611	2.03	Li I 3d to 2p	3.87-1.84	2.03
F	615	2.02	Na I 5s to 3p	4.12-2.10	2.02
G	671	1.85	Li I 2p to 2s	1.85-0	1.85
H	767	1.62	K I 4p to 4s	1.62-0	1.62
I	820	1.51	Na I 3d to 3p	3.62-2.10	1.52

Table 3. EDS measurements of powder buildup on compression hook after 2L8NS tested at 200 V/cm. Analysis comes from Figure 24. Note: Li could not be detected due to window absorption from the detector.

Scan Area	C at%	O at%	Na at%	Si at%
Spot 1	3.77	40.67	16.28	39.28
Spot 2	3.12	48.67	16.52	31.69
Overall	3.83	49.04	17.36	29.77

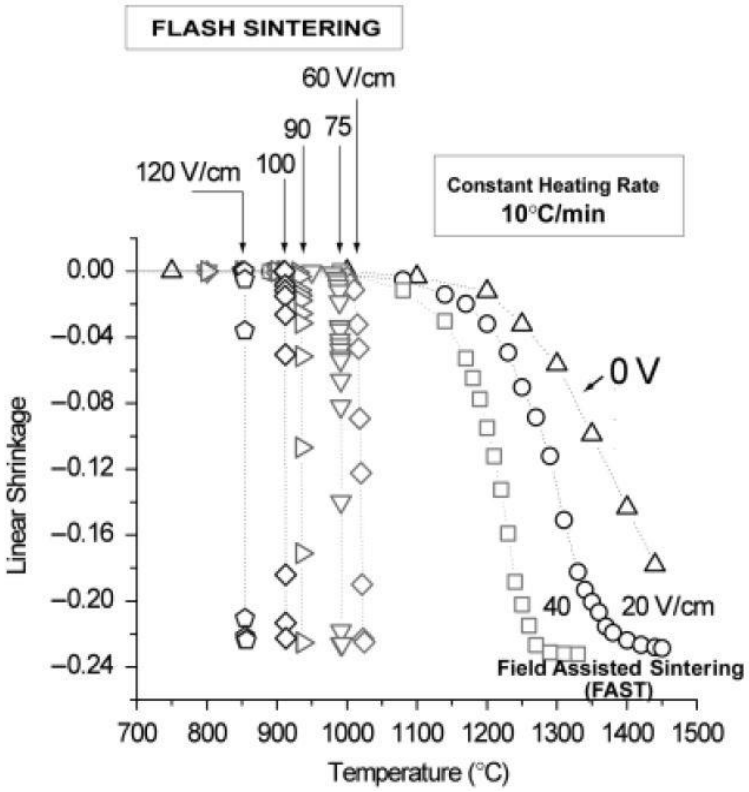

Figure 1. Enhanced sintering rates in presence of DC electrical fields for yttria stabilized zirconia showing threshold applied external electric field for flash sintering.[3]

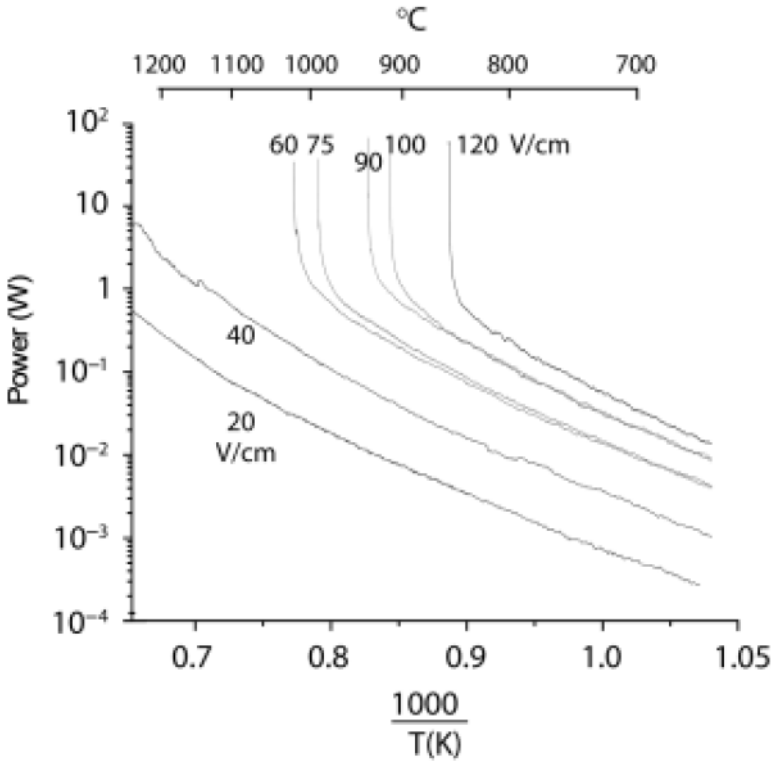

Figure 2. A power surge coincides with the onset of flash sintering when the critical sintering temperature is reached confirming that flash sintering occurs due to instability in the process.[3]

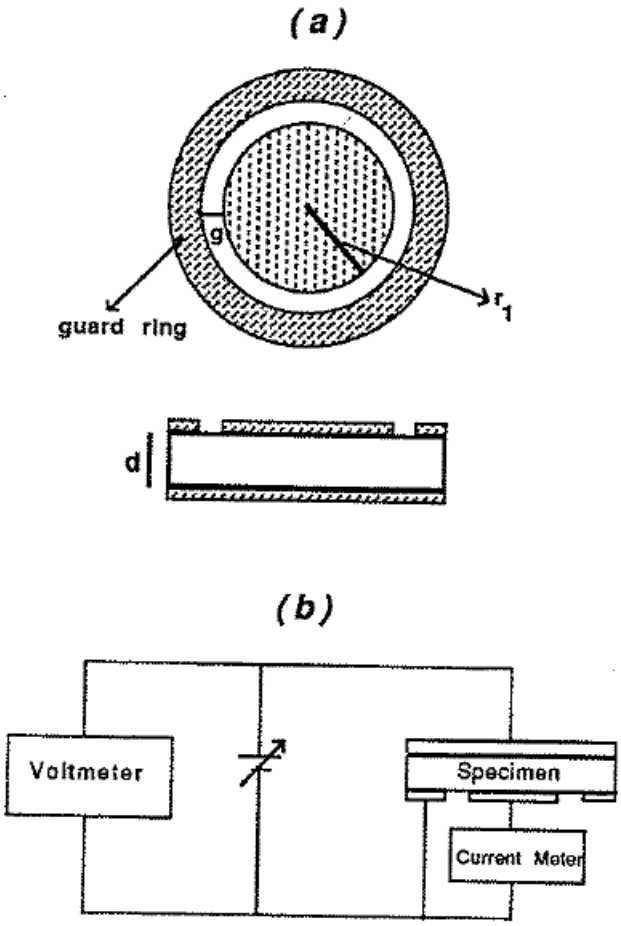

Figure 3. Three electrode configuration for electrical measurements. a) specimen with electrodes and b) circuit connections. Note: Guard ring thickness (g), central electrode radius (r_1) and sample thickness (d).[29]

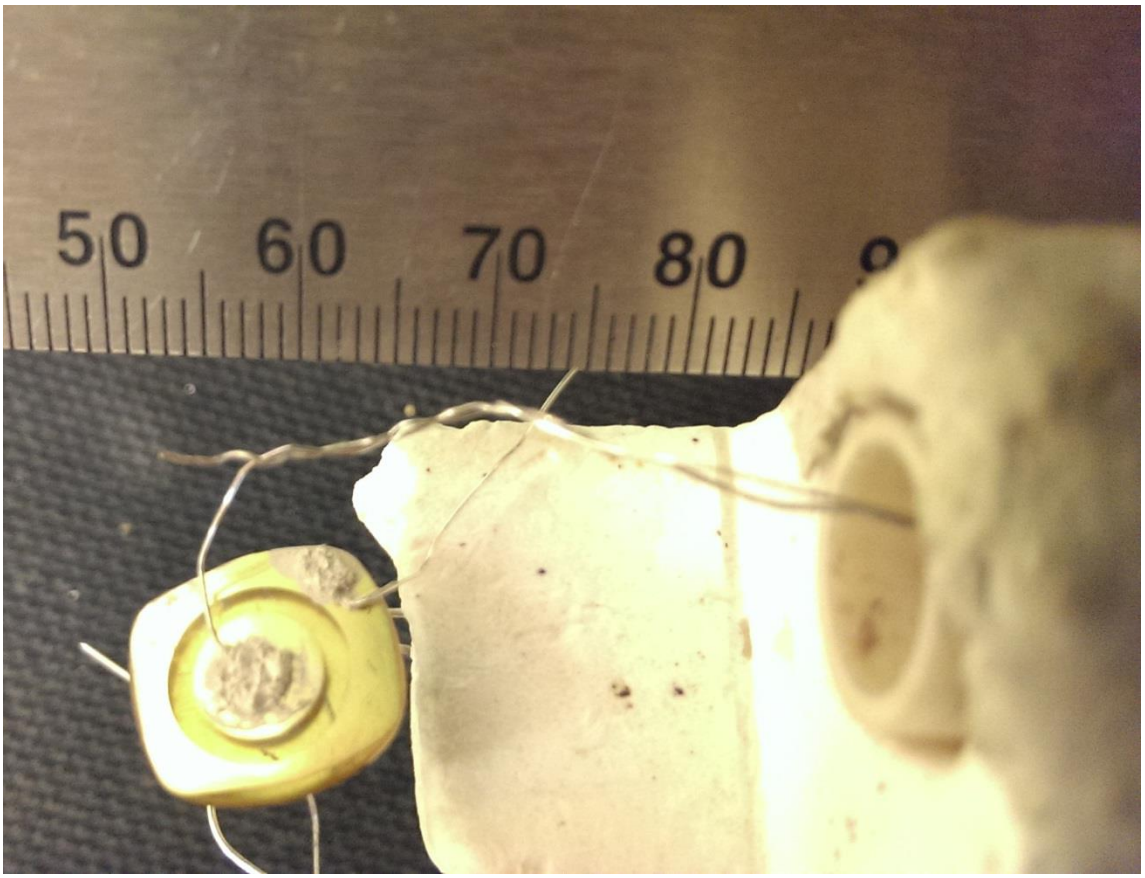

Figure 4. Image of a NS sample with gold sputtered electrodes used for impedance spectroscopy with the three-probe configuration. Top center electrode was high tension, bottom electrode was low tension and top outer electrode was ground. Gold electrodes were connected to platinum wires using silver paint.

Figure 5. Original condition of ATS pneumatic creep tester designed for tension only experiments with laser gauge to measure displacement of samples.

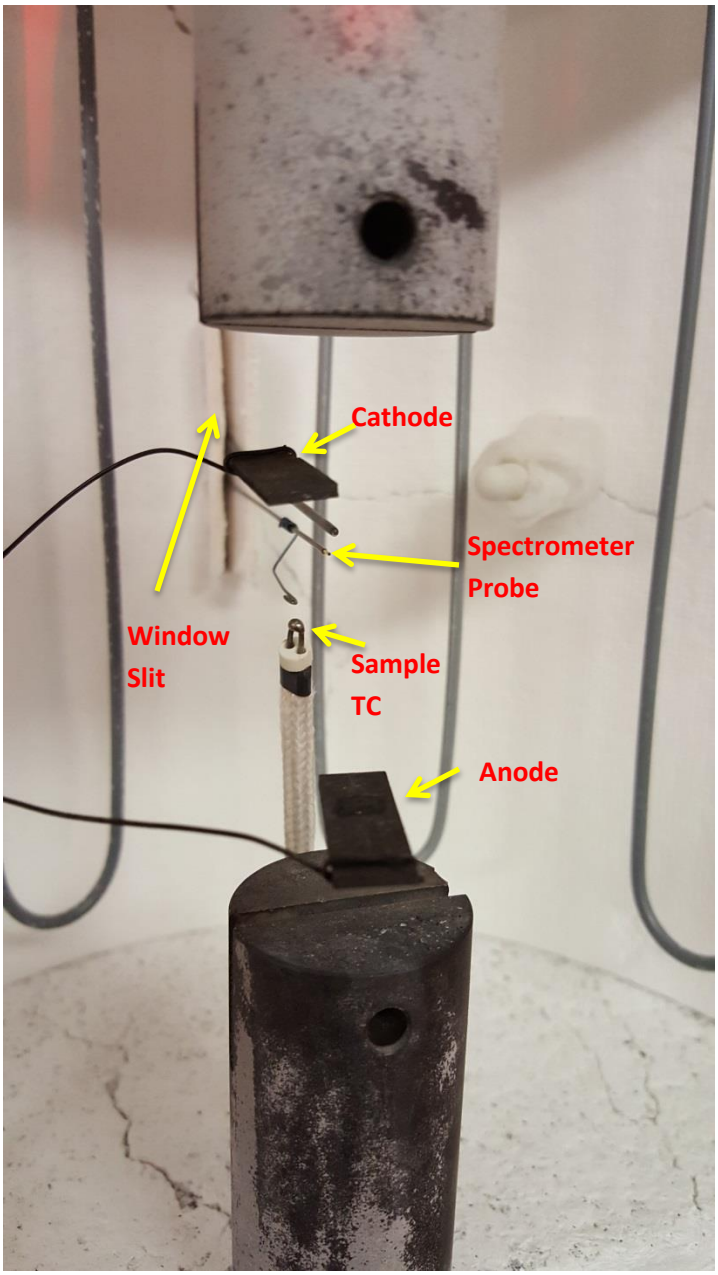

Figure 6. Modifications to ATS pneumatic creep tester for measurements of EFIS. A cathode and anode were made to apply an electric field across the sample. A spectrometer probe and video camera used the window slits into the furnace. A thermocouple (TC) was added near the sample.

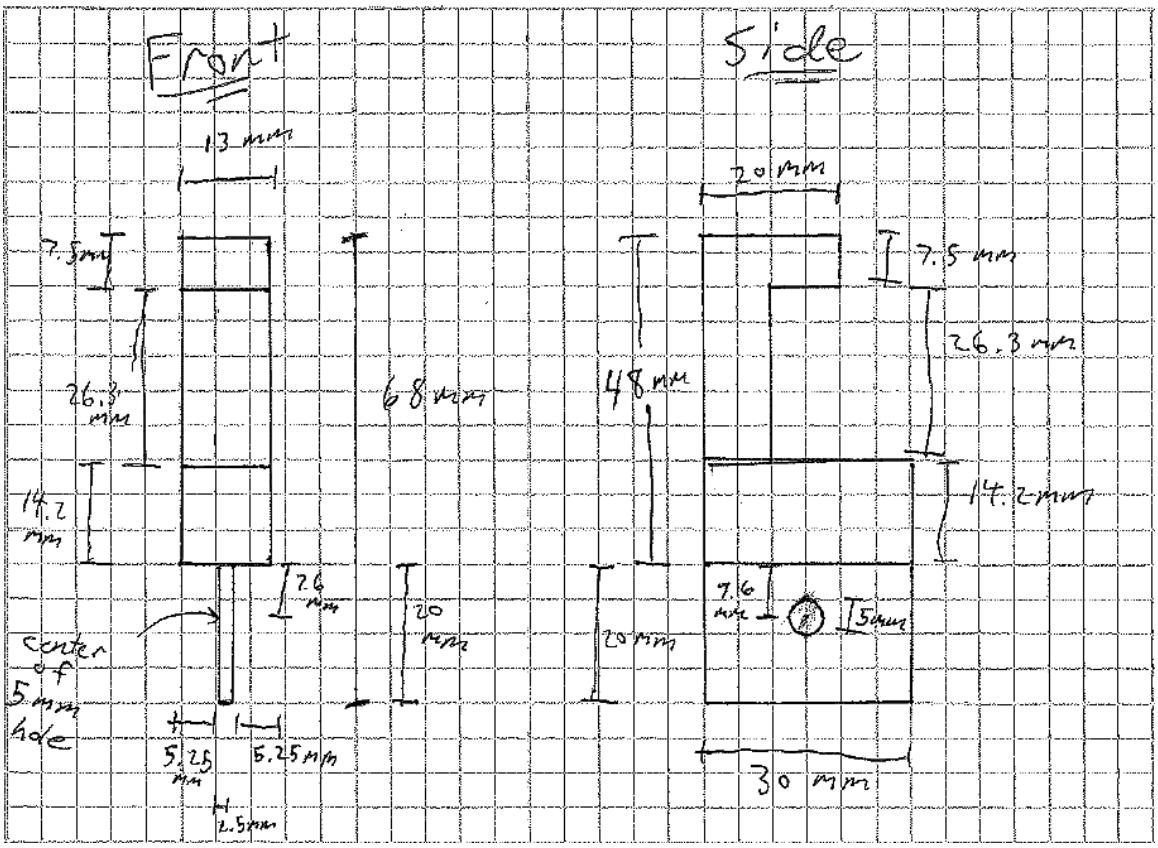

Figure 7. Design and dimensions of compressional hooks (pull to push) for application of load to glass samples in the ATS pneumatic creep tester.

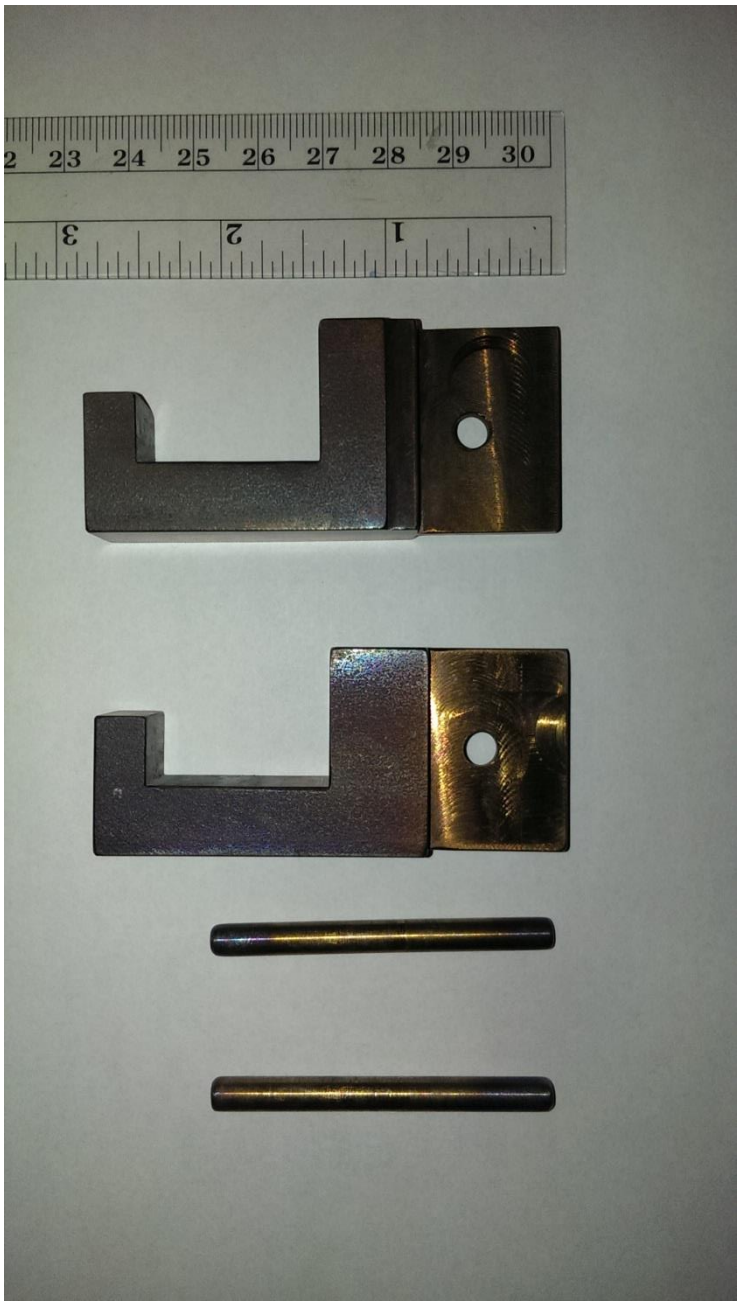

Figure 8. Machined compressional hooks following designs following the design shown previously in Figure 7.

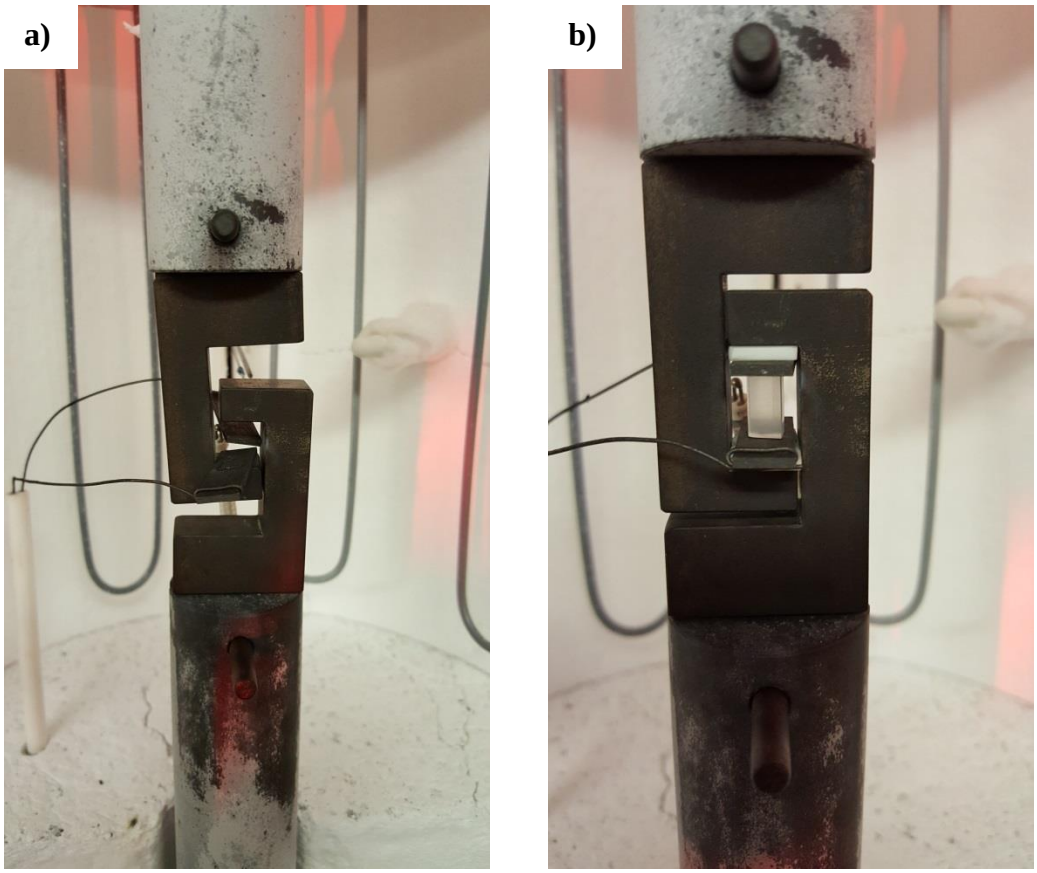

Figure 9. Images into ATS pneumatic creep tester where a) compression hooks are placed on the ends of the pull rods and b) shows sample placement between hooks.

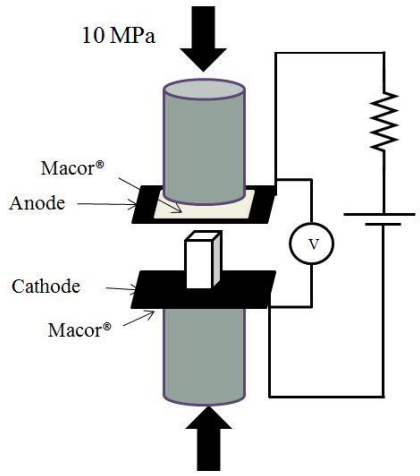

Figure 10. Experimental setup inside the modified ATS model 2605 pneumatic creep tester where the anode was located at the top of the sample and the cathode at the bottom. The system was electrically insulated from the rest of the furnace.

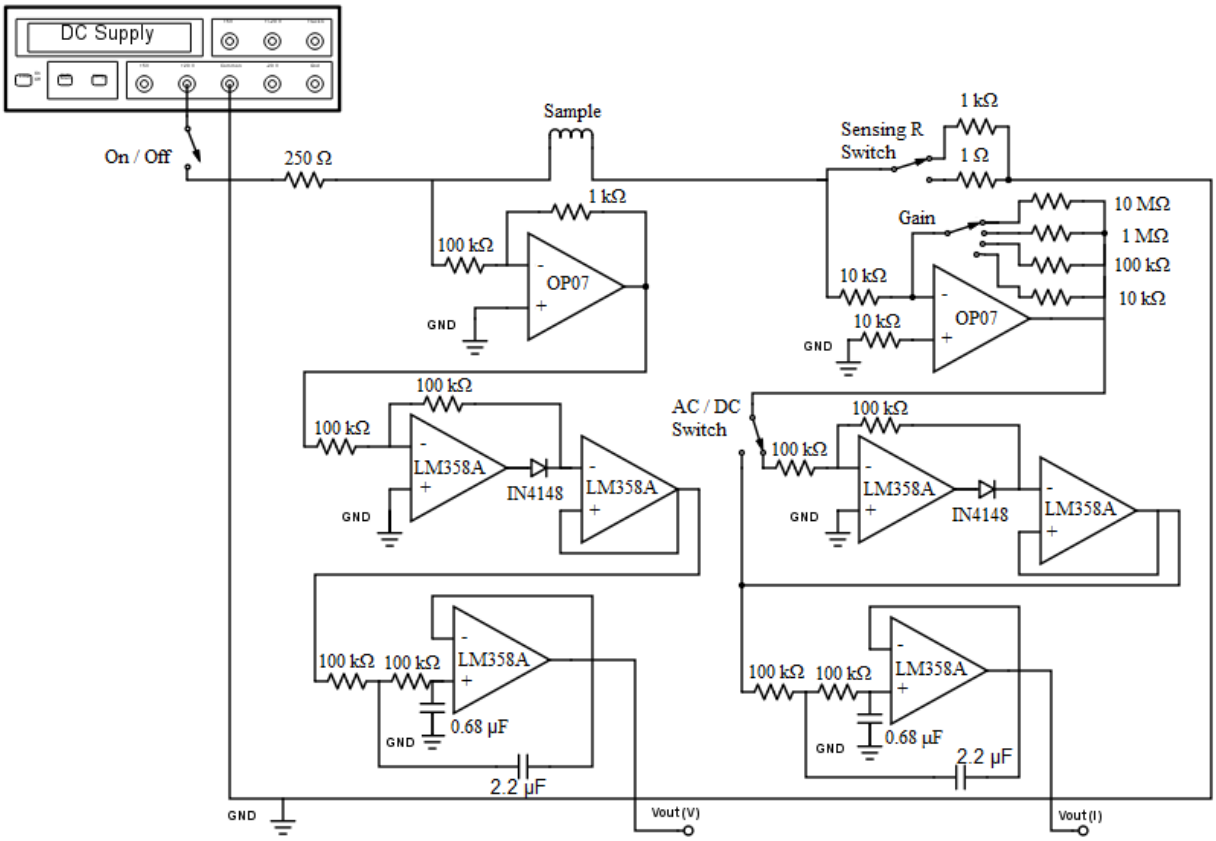

Figure 11. Schematic of measurement circuit used to record EFIS experimental data. Voltage and current were reduced and converted to 0 to 10 V DC and recorded with a DATAQ Instruments model DI-149HS.

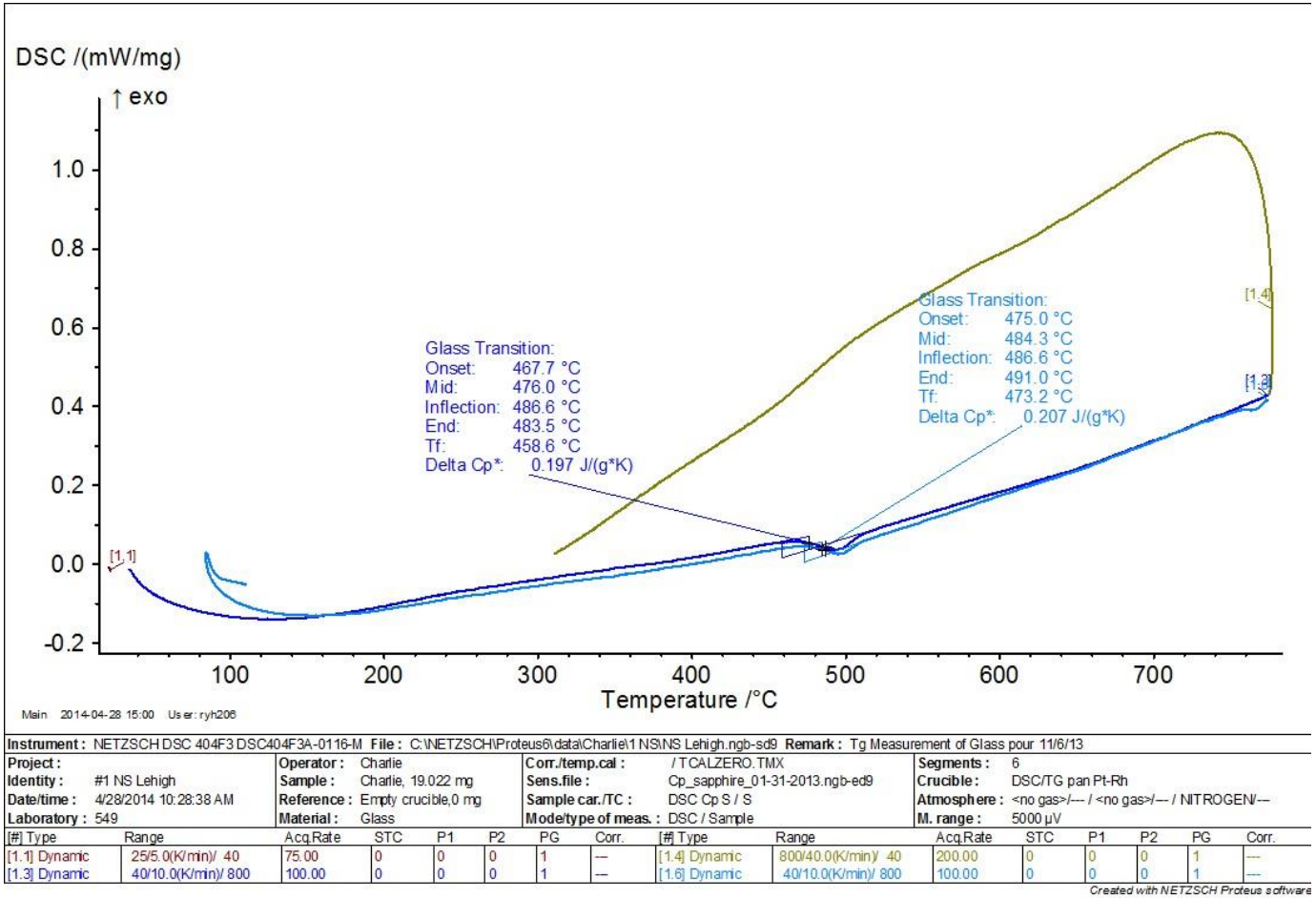

Figure 12. DSC measurement of NS from ambient to 800°C at a heating rate of 10°C/min. Tg was 475°C.

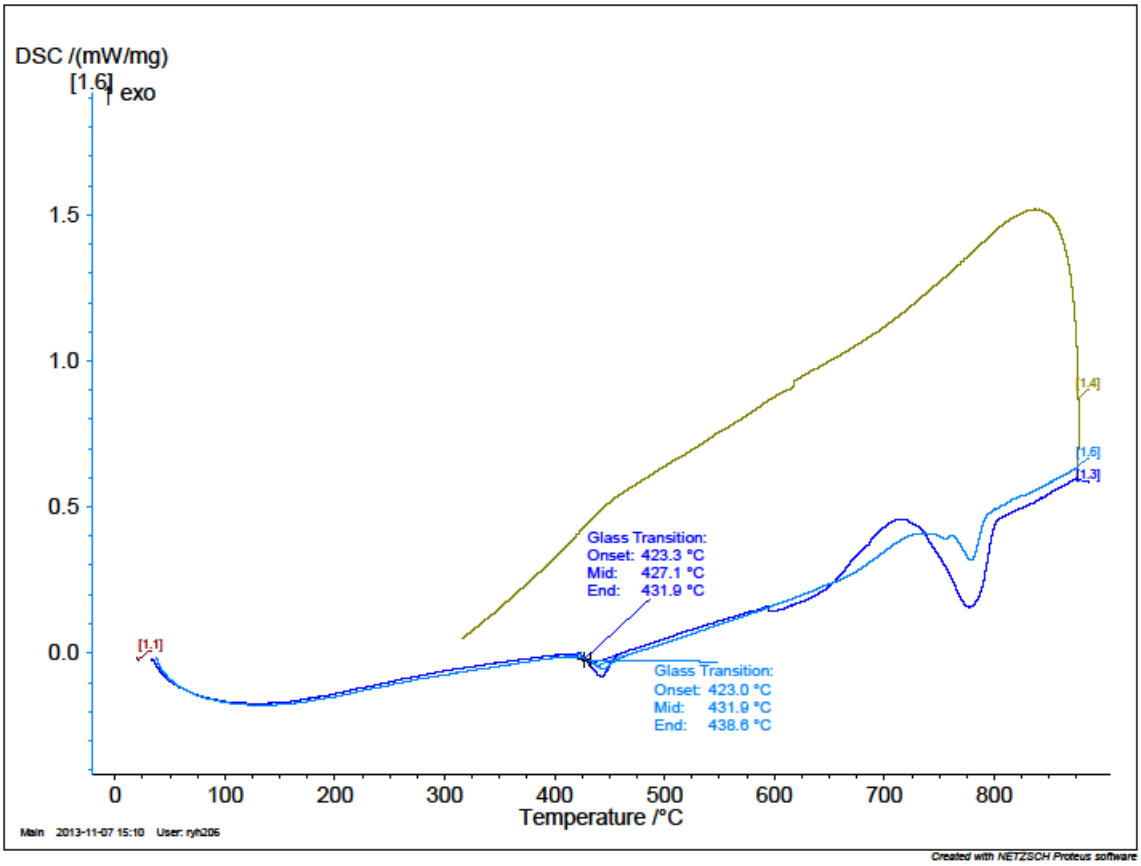

Figure 13. DSC measurement of 2L8NS from ambient to 800°C at a heating rate of 10°C/min. Tg was 427°C.

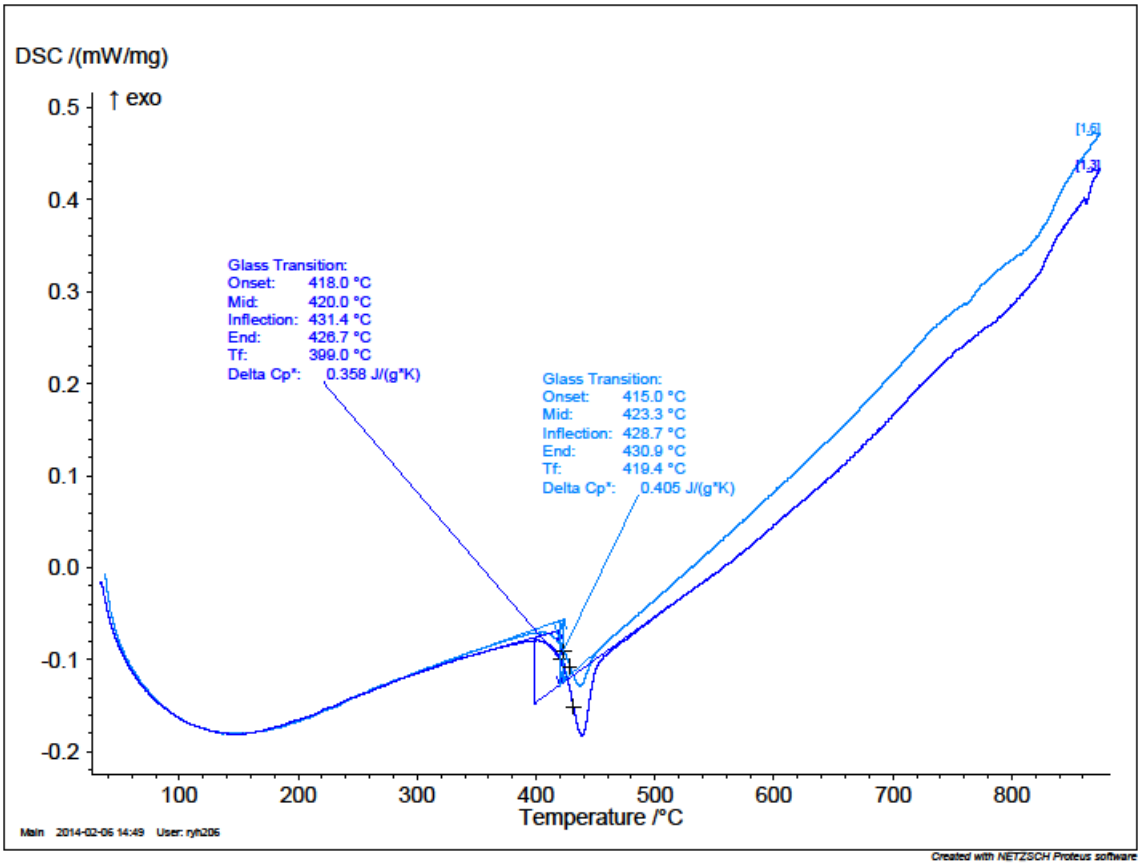

Figure 14. DSC measurement of 5L5NS from ambient to 800°C at a heating rate of 10°C/min. Tg was 423°C

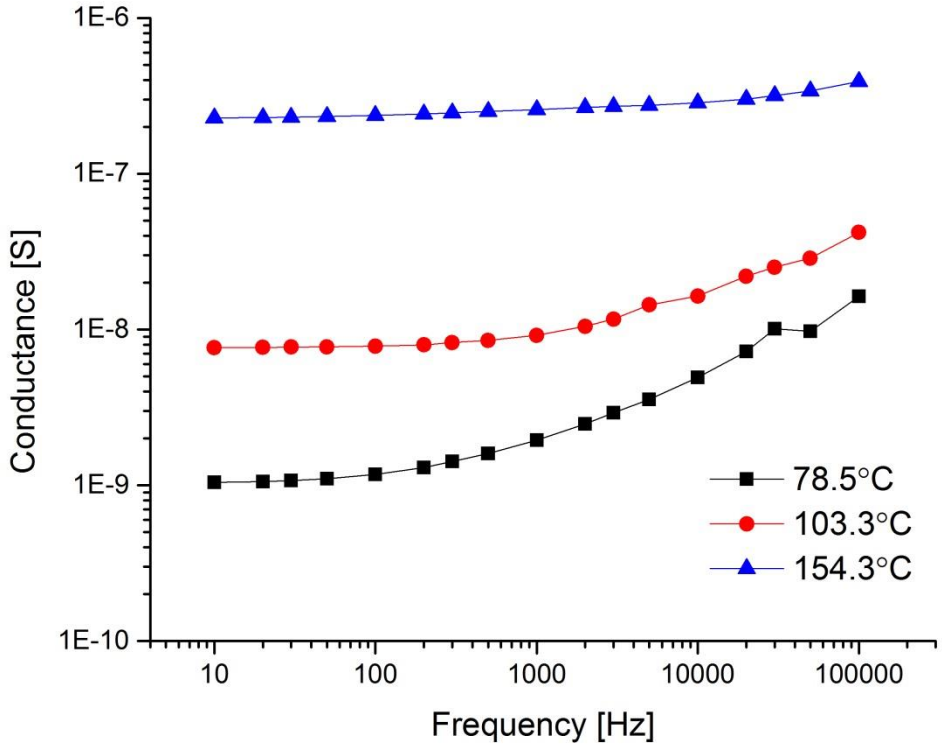

Figure 15. Representative variation of conductance vs. frequency for 2L8NS at 78.5, 103.3 and 154.3°C. Note: NS and 5L5NS compositions followed similar behavior.

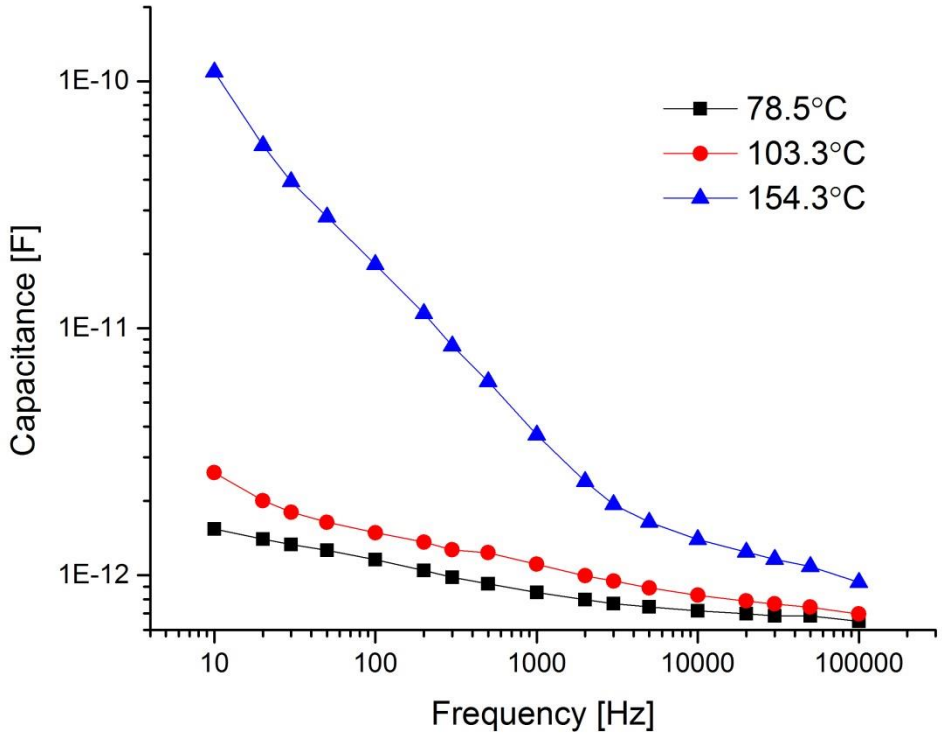

Figure 16. Representative behavior of capacitance vs. frequency for 2L8NS at 78.5, 103.3 and 154.3°C. Note: NS and 5L5NS compositions followed similar behavior.

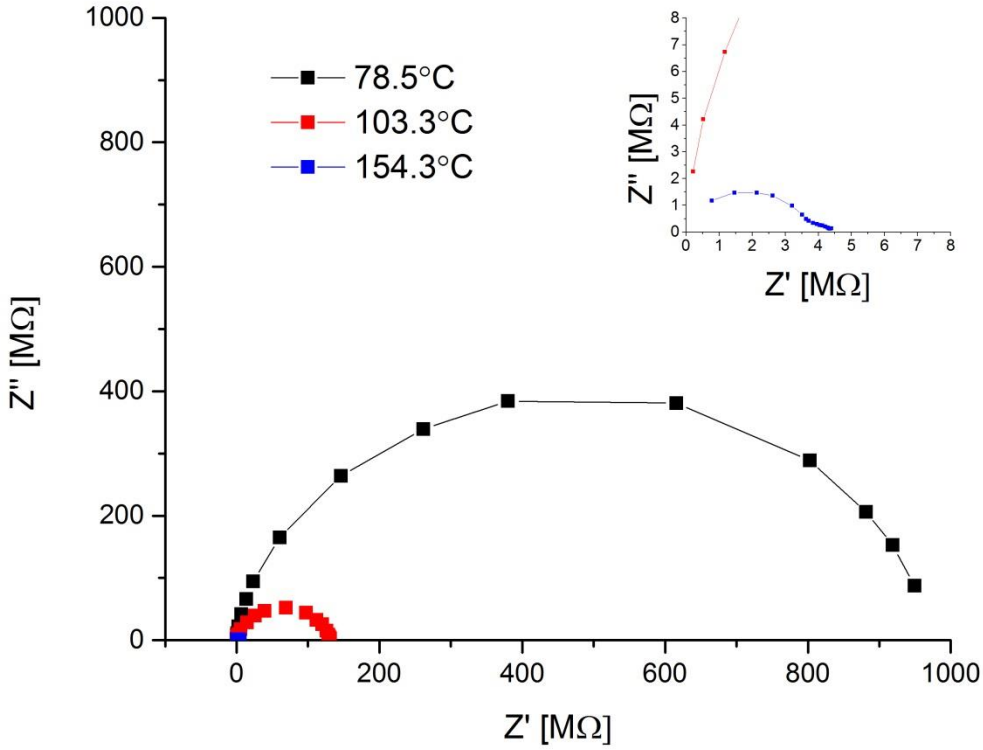

Figure 17. Nyquist impedance plots for 2L8NS at 78.5, 103.3 and 154.3°C. Real and imaginary components of impedance were calculated using data collected in Figure 15 and Figure 16. Note: NS and 5L5NS compositions followed similar behavior.

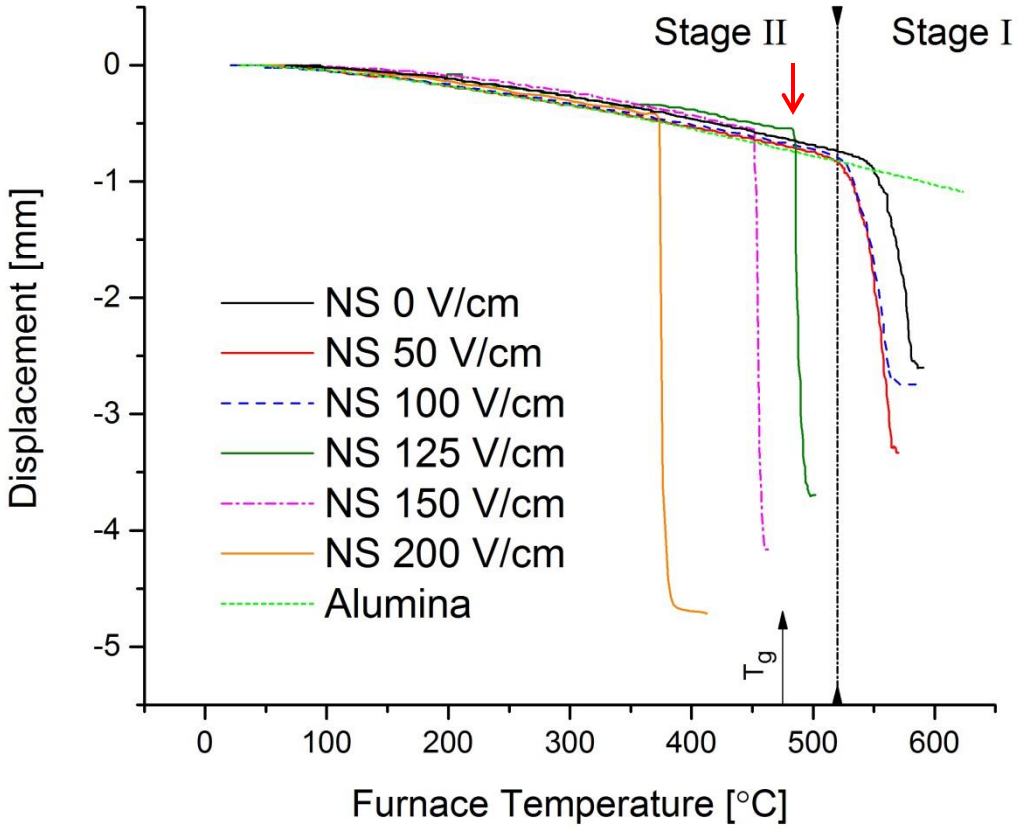

Figure 18. Displacement vs. furnace temperature of NS at various applied electric fields with a constant heating rate of 10°C/min. NS T_g indicated by arrow. Reference alumina rod displacement of support structure shown by light green dashes. Transition between Stage I and Stage II is shown by vertical line while onset of large abrupt displacement indicated by red arrow.

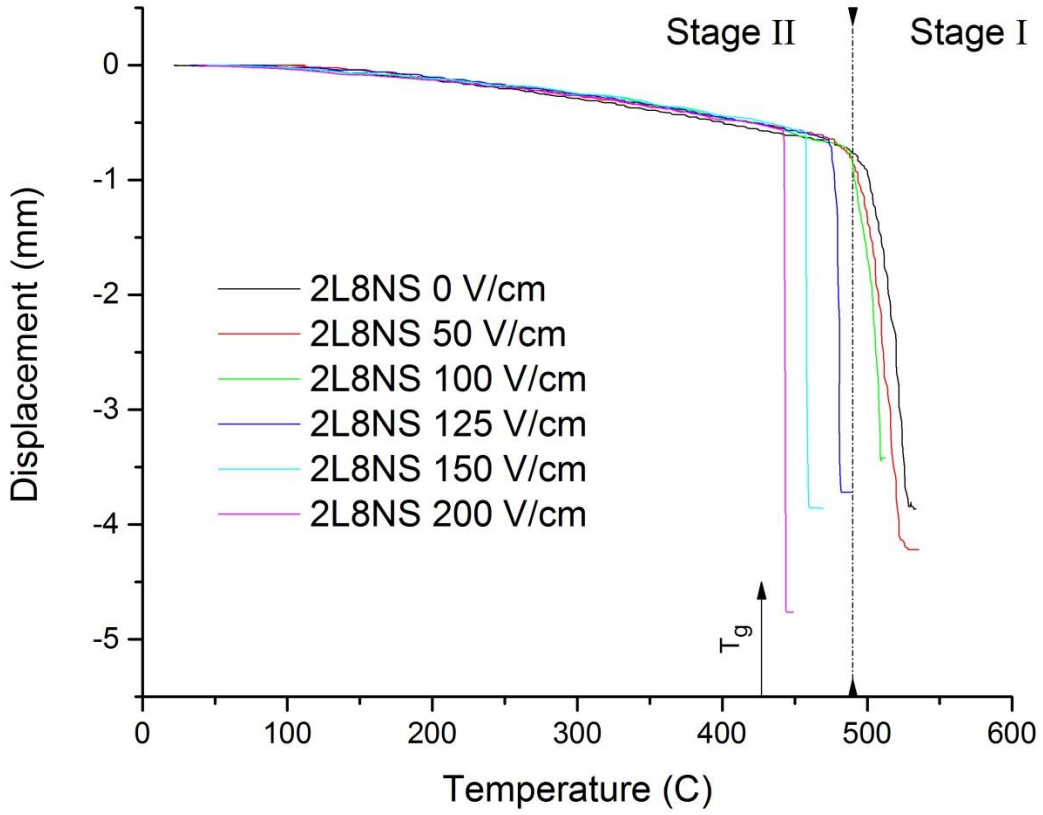

Figure 19. Displacement vs. furnace temperature of 2L8NS at various applied electric fields with a constant heating rate of 10°C/min. 2L8NS T_g indicated by arrow. Transition between Stage I and Stage II is shown by vertical line.

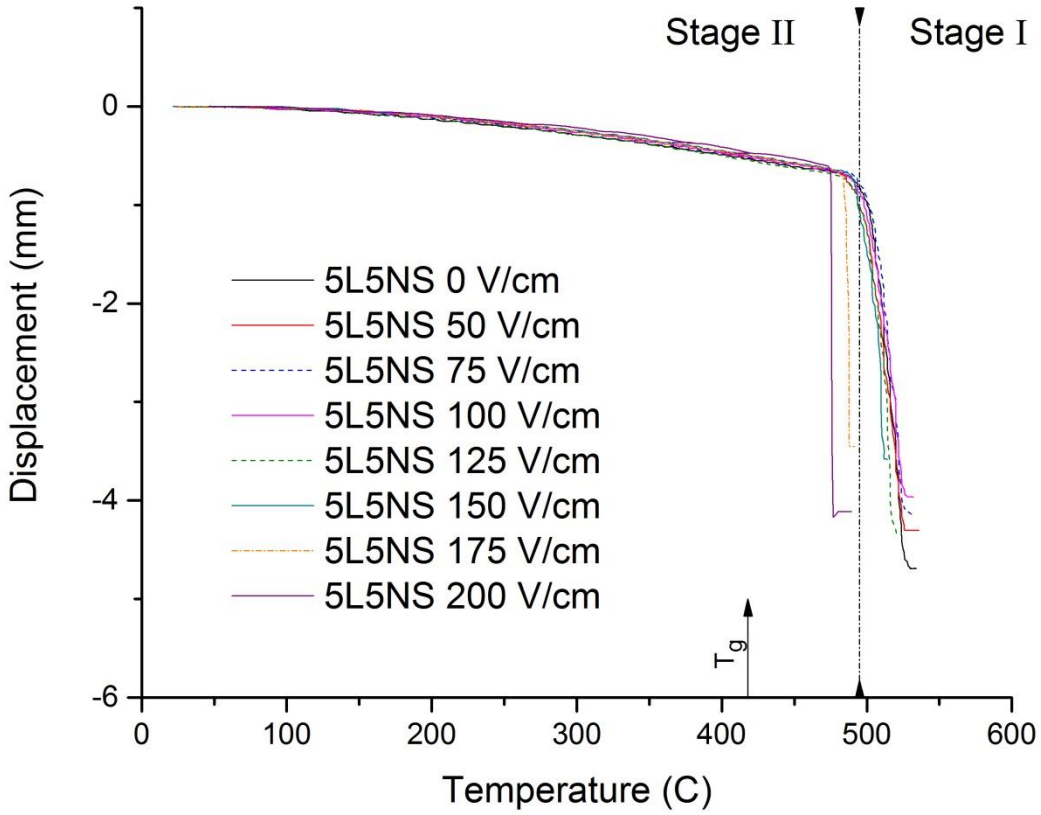

Figure 20. Displacement vs. furnace temperature of 5L5NS at various applied electric fields with a constant heating rate of 10°C/min. 5L5NS T_g indicated by arrow. Transition between Stage I and Stage II is shown by vertical line.

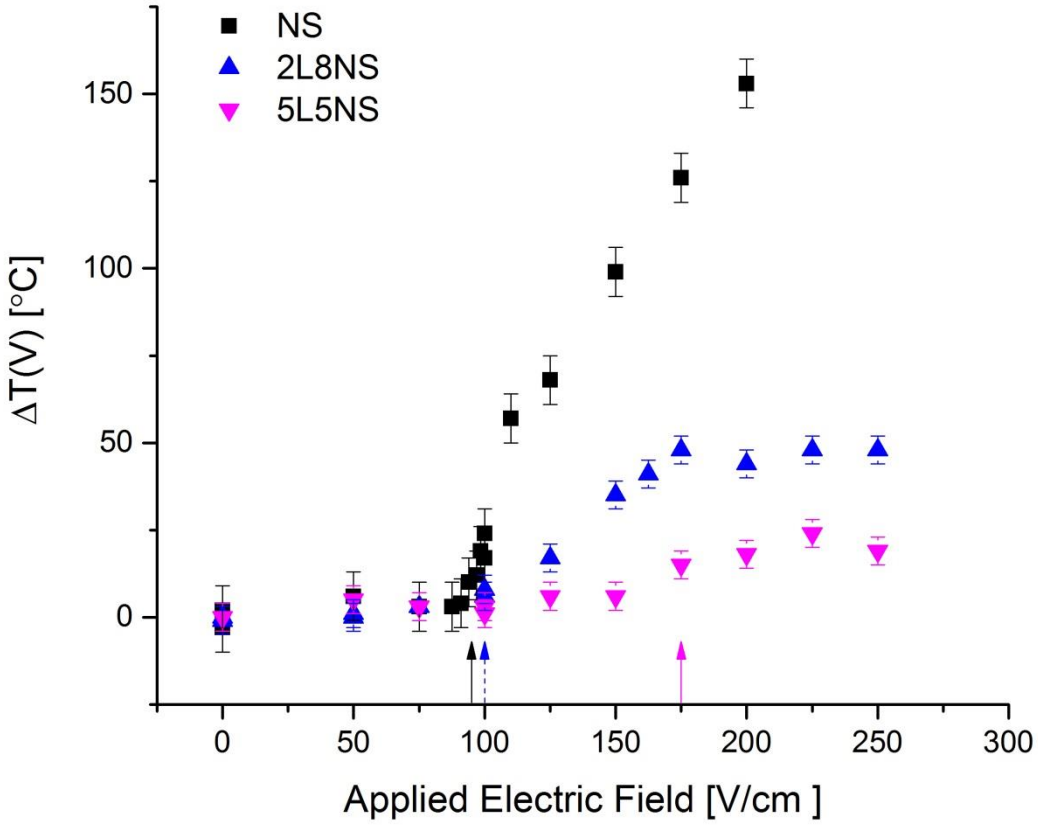

Figure 21. Normalized FIS effect for NS (black, squares), 2L8NS (blue, triangles) and 5L5NS (pink, inverted triangle). The Difference ΔT(V) in regular softening temperature (T_{s0}) to softening temperature with an applied electric field (T_{sV}) plotted versus applied electric field. Arrows indicate approximate threshold applied electric field for each glass composition.

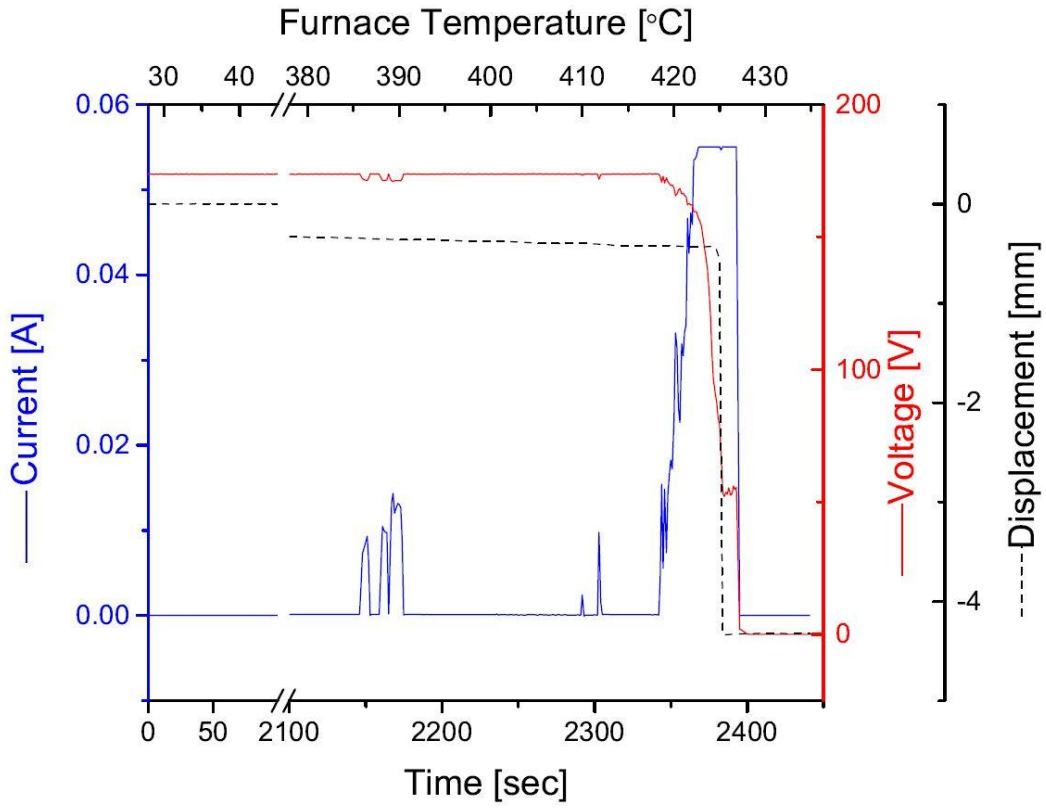

Figure 22. Time dependence of current (blue, solid), voltage (red, solid) and displacement (black, dashed) for NS under the application of 175 V/cm field at a heating rate of 10°C/min. Note: Current amplifier became saturated during high current regime.

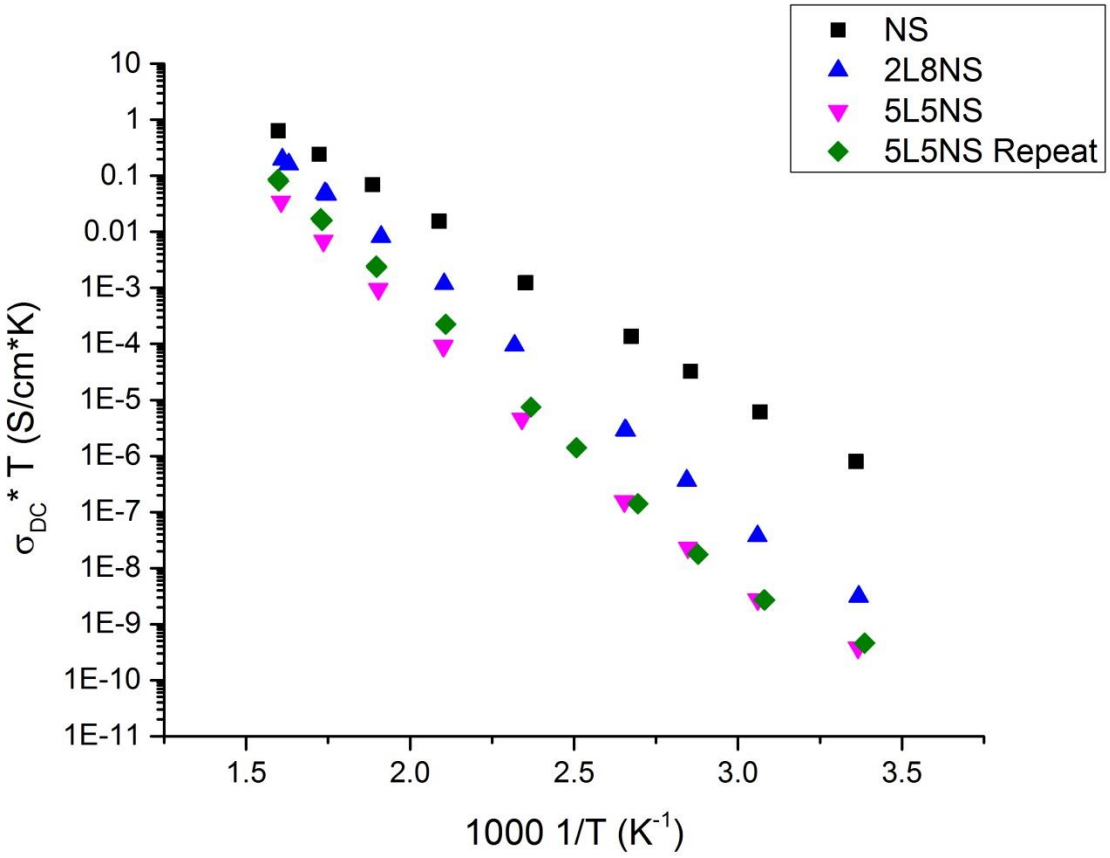

Figure 23. Arrhenius plot for activation energy for each glass composition using impedance spectroscopy ranging from ambient to about 400°C

a)

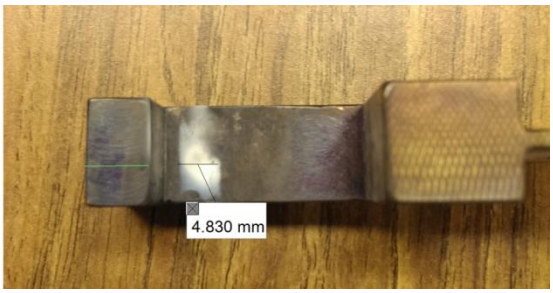

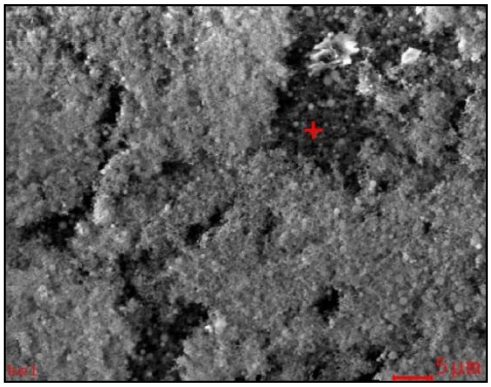

b)

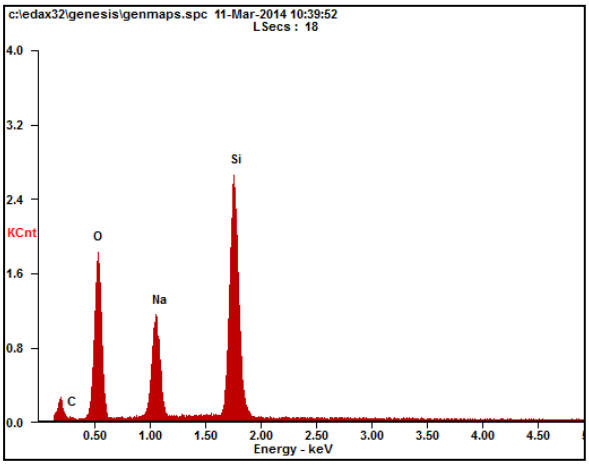

c)

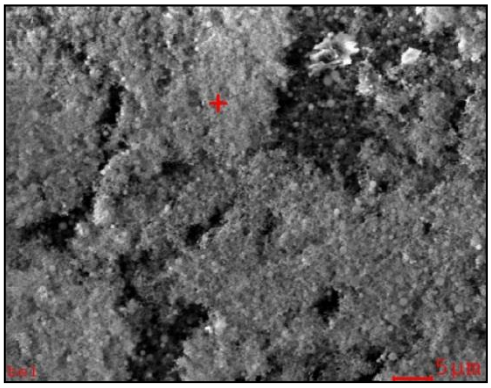

d)

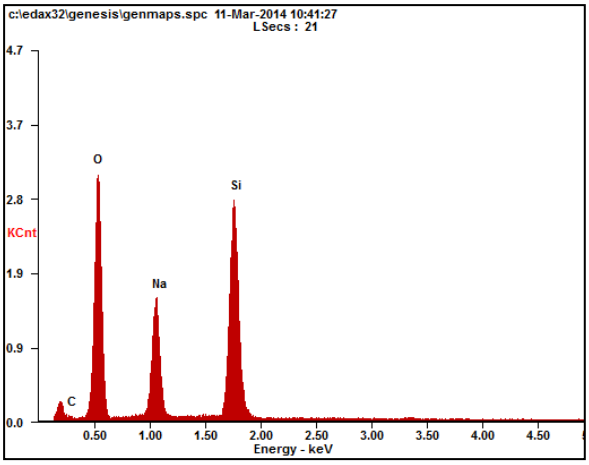

e)

Figure 24. After testing 2L8NS with 200 V/cm a) buildup of white powder was observed on the compression hook near the anode. The powder was investigated using EDS where b) spot 1 is indicated by the red crosshairs with its c) collected spectrum and d) spot 2 again indicated by the red crosshairs with its e) collected spectrum. The semi quantitative compositions are given in Table 3.

a)  **b)** 

Figure 25. Images of NS during 150 V/cm test condition when the furnace temperature was a) $T<T_F$ and b) $T_F<T<T_S$ of EFIS.

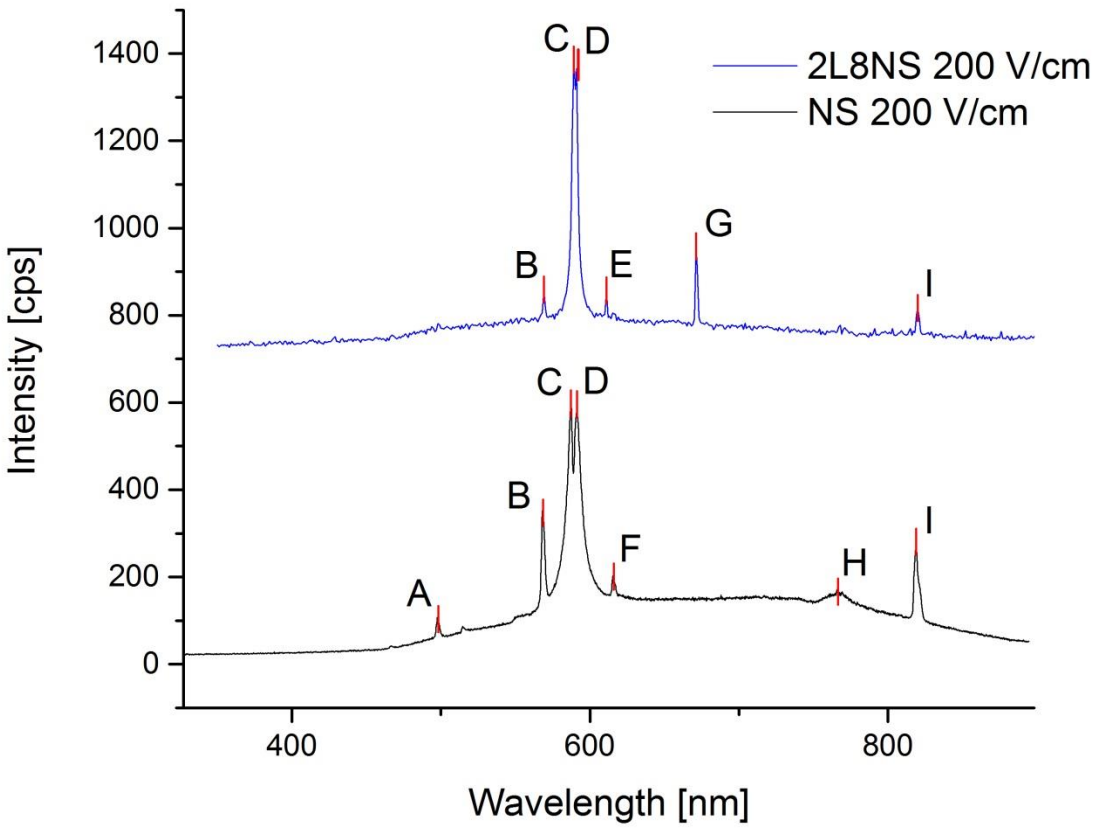

Figure 26. Photoemission spectra at the 200 V/cm test condition ranging from 350-900 nm for NS (black, bottom) and 2L8NS (blue, top). Peaks labels correspond with those listed in Table 2. 5L5NS has same peaks as 2L8NS. Note: Intensity of 2L8NS was offset by an arbitrary amount for comparison.

Appendix A

Impedance Spectroscopy Testing Procedure

1. Make sample disk by grinding and polishing to a 400 grit surface finish where the sample thickness is ~2mm or less
    a. The thinner and wider a sample will give less noise in the data
2. Cover edges of sample with carbon tape then sputter gold on the entire bottom surface
3. Then flip sample over, place washer on top surface of sample and sputter gold again.
    a. The washer is used to create a guard ring for grounding the sample
    b. Three electrode configuration
        i. High Tension – Top middle
        ii. Low Tension – Bottom
        iii. Ground – Outside Top
4. Clean wires with acetone before attaching to setup
5. After attaching the sample to the setup, place setup inside alumina tube of furnace
    a. Make sure mark on tube lines up with the edge of the furnace
    b. Hook up thermocouple to fluke meter
    c. Connect ground to the ground wiring on the back of the setup
6. Turn on temperature control and adjust temperature control manually with excel calibration file
7. Turn on Andeen capacitance bridge
8. On the computer, open Microsoft Advanced Basic for conductivity testing

    a. F3 to load a program
        i. LOAD”c:\basic\bridge_c”
        ii. Enter
    b. F2 to run program
        i. Ask which communication port
            1. 2 -> Enter
9. Set bridge by hitting reset -> 6 -> 1
    a. Press enter to send test command to see if bridge is reading correctly
10. Press enter to send command and continue
11. Enter # of samples
12. Enter output file name
    a. Example.out
        i. Saves to c:\basdata
13. Program asks if you want to redefine output file name
    a. Enter to continue if satisfied with name
14. Press 2 to run a measurement and hit enter
15. Enter command **F04G6** in uppercase for frequency sweep
16. Enter starting temperature [C] to start test
17. Enter end temperature [C]
    a. Usually do 3 measurements per temperature step for statistics
18. When done with all measurements press 4 then hit enter to exit Basic
19. Then type SYSTEM and hit enter to close window
20. Turn off Andeen capacitance bridge when done

Appendix B

Field Assisted Viscous Flow Testing Procedure

1. Record dimensions and mass of test specimen in 3rd floor lab
2. Turn on ATS Creep Tester and furnace controls with front two main switches
3. Apply carbon paste to top and bottom of the test specimen
    a. Wipe excess paste off with Kimwipe and let dry
4. Load DATAQ Instruments Hardware Manager
    a. In edit menu change sampling rate to 1 point/sec or faster
    b. Also add channels 5, 6 and 7
5. Open Excel template for data collection
    a. While waiting for both programs to open record starting TARE cylinder value
6. In Excel fill in the cells that are highlighted yellow and save file as #Glass Type and Field
    a. From height dimension calculate the voltage needed to be applied to achieve the desired field [V/cm]
7. If needed, replace graphite electrodes or Macor® by removing the pins from the compression C-hooks from the pull rods.
    a. If a new electrode is needed, cut graphite using low speed saw to 1.75mm thick X 8mm wide X 14mm long. Then two grooves need to be filed near to end of one long dimension in order to hold the copper wire loop in place.

b. If new Macor® is needed, cut Macor® to the dimensions that will cover most of the space between the opening of the two C-hooks for top and bottom. This can easily be done using a hacksaw and vice with a piece of wood.
c. Place the C-hooks back on the pull rods

8. Set ATS creep Tester to LOAD
9. Open the air valve slightly in order to let enough air pressure to raise the bottom pull rod. Builds up to 30 lbs then wait until the applied pressure returns to zero or near zero on readout screen.
10. Once bottom pull rod has reached the top (Think of this as building from bottom to top for the sample setup), place a piece of Macor® on the bottom C-hook.
    a. Then place the graphite cathode on top of the Macor®.
    b. The sample is then placed standing up with the graphite paste in contact with the graphite electrode.
    c. The reverse is done for the top where the anode is in contact with the top of the sample.
    d. The top Macor® piece then is placed to separate the electrode from the C-hook.
11. When finished, hold the setup steady with your left hand and then apply 4lbs of pressure using the thumbwheel. This will cause the bottom pull rod to move downwards and hold the setup itself.
12. Then open the air valve a little more in order to apply <30 PSI

13. When the air pressure is steady, apply 7lbs in order to force good contact between electrodes and sample.
14. Now time to check the voltage; turn on the DC power supply and turn the knob on the front so the voltage is 15V. Check using blue multimeter and charge if necessary.
    a. Turn the circuit switch to ON and then check the voltage between the electrodes. Also check the voltage between each electrode and each C-hook to make sure it is zero or very small. (We don't want to have stray potentials)
    b. If there are any stray voltages on the C-hooks adjust the electrodes and wire leads from touching the C-hooks
15. Once the voltages are fine, increase the DC power supply to the desired applied voltage
16. Then increase the pressure (cross section x 10 = N) to 59lbs (250N) and close the furnace door. Make sure to close the four latches around the furnace starting with the bottom two.
    a. Then adjust the fiberfrax insulator around the bottom pull rod and the bottom of the furnace opening.
17. Now connect the two batteries to the data collection circuit and check their values in DATAQ
    a. I recommend doing a test run in Excel before actually starting the test just to make sure everything is collecting properly.

b. Start a test run by going to the Add-Ins menu and clicking on the left button called start Windaq-XL
c. In Device settings tab select DI-149. In Import Options tab select Time Stamp, Starting cell B7 and Rows to Fill 6000 and Select save Settings.
d. Once these are filled out hit Start Import.
e. If test numbers are good then stop data collection with the square stop button

18. Set the furnace controls to proper heating rate and setpoint (Usually 10°C/min to 620°C)
19. Before starting the furnace make sure that:
    a. Voltage is on
    b. Correct pressure is applied (Typically 59lbs, 250N, 10MPa for 5mm X 5mm sample cross section)
    c. Furnace is set
20. On the furnace control press start and change to auto mode.
21. Once the temperature of the furnace begins to rise, start the data collection and record the starting temp.
22. After the data collection has started, click and drag the time reference cell (J31) to cell (I31) and double click bottom right corner of cell to extend to bottom of column.
    a. This is only needed if you want to see the graphs plotted in real time (I recommend this)

23. If video is to be collected, setup the camera on the tripod with the legs placed on the masking tape on the floor.
    a. Will not be able to see into furnace until blackbody radiation is great enough around 400°C
    b. Start recording video before significant deformation or flash occurs and record which cell the video recording started (This will help sync the data to video)
24. If the photoemission is to be collected, open OceanView software in quick view
    a. Setup the save configuration to save in a folder for the test run after every 5 scans.
    b. Add save directory with new folder then label the basename with the 5 padding digits
    c. Press the save spectrum button before expect photoemission occurs

End of Test Procedure

1. After the test has completed, the first thing should be to switch the voltage OFF using the circuit switch
2. Let the data collection continue for a few more seconds and then press the square stop button
    a. SAVE DATA with new file name than the template excel sheet.
    b. Stop photoemission collection
    c. Stop video recording (If cell wasn't marked when video started, sync to when voltage was turned off if flashing occurred)

3. Then the furnace should be turned off manually by pressing the manual mode button on the furnace control. Then slowly decrease the output% down to zero and press the start/stop button. (It is a good idea to do this manually because it will lead to a longer lifetime of the heating elements inside the furnace)
4. Next, dial down the voltage of the power supply slowly. Once the voltage is zero turn off the power supply.
5. Then decrease the applied pressure using the thumbwheel by setting it to zero.
    a. The creep tester will take a few moments to release the pressure
    b. Also make sure to record the ending TARE cylinder pressure
    c. Unhook batteries
    d. Turn off blue multimeter
6. When the furnace has cooled to about 350°C the air valve can be closed
    a. Unlatch the furnace door and open slightly to remove the Macor® pieces using the tweezers and place on bottom of furnace and close the furnace door
    b. To dump tare cylinder set the ATS Creep Tester to SETUP and turn the leftmost handle to dump tare pressure
    c. The Video can then be copied over from the camera to the desktop and SAVED
7. Let the furnace continue to cool down naturally (This will take a little bit more than an hour)
    a. Once the furnace has cooled to ~70°C the furnace door can be opened again and the sample can be taken out

b. A good portion of the time the sample sticks to the top electrode and needs to be carefully detached in order to not break the glass sample
c. Once sample is removed place top of sample towards the front of the sample bag and close the furnace door for consistency

8. Turn off power for ATS Creep Tester and furnace controls with front two main switches

Vita

Charles Thomas McLaren was born and raised in Corning, New York by his parents George and Susan McLaren. He attended Erwin Elementary School, Northside Blodgett Middle School, and Corning – Painted Post West High School, from which he graduated in 2008. In August, 2008 Charles enrolled in Rutgers University in New Brunswick, New Jersey where he majored in Materials Science and Engineering with a focus on ceramics and glass. He graduated with highest honors and received a Bachelor of Science degree in May 2012. Charles then chose to continue his education by enrolling in the graduate degree program at Lehigh University in the Department of Materials Science and Engineering, where he joined the International Materials Institute for New Functionalities in Glass (IMI-NFG) under the advisement of Dr. Himanshu Jain. He graduated with his Master of Science degree in May 2016 and is continuing on toward his Ph.D.